https://doi.org/10.5194/gmd-2024-26
Preprint. Discussion started: 2 May 2024

Geoscientific Model Development Discussions

BOATSv2: New ecological and economic features improve simulations of High Seas catch and effort

Jerome Guiet [1], Daniele Bianchi [1], Kim J. N. Scherrer [2], Ryan F. Heneghan [3], and Eric D. Galbraith [4]

[1]Department of Atmospheric and Oceanic Sciences, University of California Los Angeles, Los Angeles, CA, United States
[2]Department of Biological Sciences, University of Bergen, 5020 Bergen, Norway
[3]School of Science, Technology and Engineering, University of the Sunshine Coast, Petrie, Australia
[4]Earth and Planetary Science, McGill University, Montreal, QC, Canada

Correspondence: Jerome Guiet (jerome.c.guiet@gmail.com)

Abstract. Climate change and industrial fishing have profound effects on marine ecosystems. Numerical models that capture key features of fish biomass dynamics and its interaction with fishing can help assess the biogeochemical and socio-economic consequences of these impacts. However, these models have significant biases and do not include many processes known to be relevant. Here we describe an updated version of the BiOeconomic mArine Trophic Size-spectrum (BOATS) model for global fish and fisheries studies. The model incorporates new ecological and economic features designed to ameliorate prior biases. Recent improvements include reduction of fish growth rates in iron-limited high-nutrient low-chlorophyll regions, and the ability to simulate fisheries management. Novel features described here include a separation of pelagic and demersal fish communities to provide an expanded representation of ecological diversity, and spatially variable fishing costs and catchability for more realistic fishing effort dynamics. We also introduce a new set of observational diagnostics designed to evaluate the model beyond the boundary of large marine ecosystems. Following a multi-step parameter selection, the updated BOATSv2 model shows comparable performance to the original model in coastal ecosystems, accurately simulating catch, biomass and fishing effort. The revised model provides a markedly improved representation of fisheries in the High Seas, largely correcting the biases of the original version, including excessive high-sea catches and too rapid deepening of fishing effort over time. The updated model code is available for simulating both historical and future scenarios.

1 Introduction

Recent theoretical and empirical developments have enabled the development of size-based fish community models based on fundamental ecological principles (Heneghan et al., 2021). Instead of explicitly representing linkages between species or functional groups in food-webs, aggregated size-spectrum models are founded on properties that emerge at higher levels of organization, relying on macroecological principles to connect individual growth and metabolism (Brown et al., 2004; Kooijman, 2010; Hatton et al., 2021) to community level production and biomass (Gascuel et al., 2011; Blanchard et al., 2012; Maury and Poggiale, 2013; Jennings and Collingridge, 2015; Petrik et al., 2019; Heneghan et al., 2020). By simplifying complex ecosystems dynamics into community-level biodiversity (Maury, 2010; Petrik et al., 2019) and regional variations in trophic efficiency (Du Pontavice et al., 2020) and other ecological variables, these models can project the response of global

https://doi.org/10.5194/gmd-2024-26
Preprint. Discussion started: 2 May 2024


Geoscientific Model Development Discussions

marine ecosystems to warming and shifts in primary production due to climate change (Lotze et al., 2019; Tittensor et al., 2021).

The BiOeconomic mArine Trophic Size-spectrum (BOATS) model is a size-spectrum model that incorporates an explicit representation of commercial fishing effort (Carozza et al., 2016, 2017). The model's integration of ecological and economic dynamics enable a clear illustration of the profound effects of advances in fishing technology on historical changes in fish biomass, as compared to the impacts of climate change (Galbraith et al., 2017; Carozza et al., 2019). The ability to simulate how fish catches respond to dynamic fishing effort allow optimization of the model's ecological parameters against observational reconstructions of large-scale fish catches (Carozza et al., 2017). Based on this optimization method, BOATS provided new estimates of the global biomass and cycling rate of fish, indicating a non-negligible impact of fishing on carbon sequestration and biogeochemical cycles (Bianchi et al., 2021; Le Mézo et al., 2022), and providing mechanistic insights on the historical progression of fisheries (Guiet et al., 2020). While the model was originally designed under the assumption of open-access fishing effort, subsequent developments enabled it to investigate the effects of regulatory measures on fish community dynamics and their response to long-term and abrupt climate perturbations (Scherrer and Galbraith, 2020; Scherrer et al., 2020).

While BOATS has proven useful for exploring multiple aspects of global fisheries dynamics, comparisons with observations have also revealed discrepancies that suggest missing mechanisms. For instance, comparison with global fishing effort reconstructions suggested excessive fishing activity in iron-limited high-nutrient low-chlorophyll (HNLC) regions (Galbraith et al., 2019). Similarly, while the model provides a realistic representation of coastal fisheries, catches in the High Seas (here defined as the regions of the ocean beyond Large Marine Ecosystems) appear to be much larger than recent observational reconstructions. Specifically, BOATS simulates 40% of global catches beyond the boundary of Large Marine Ecosystems (LMEs) by the 1990s. This is approximately four times larger than the value of $8-9\%$ from empirical estimates (Watson, 2017; Pauly et al., 2020). The large High Seas catches coincide with excessive fishing over deep seafloor. During the 1990s, the model's catch-weighted mean depth of fishing is 1698m, contrasting significantly with the observational reconstructions range of $154-372$m. This discrepancy limits the model's applicability to study the interaction of industrial fishing with High Sea and deep-ocean ecosystems, and suggests potential shortcomings in the representation of open-ocean food webs.

In parallel, recent studies have shed new light on large-scale aspects of global marine ecosystems and fisheries. Reconstructions of industrial fishing effort by Global Fishing Watch (GFW, Kroodsma et al. (2018)) highlighted spatial variations in fishing costs (Sala et al., 2018) and revealed the importance of seamounts in concentrating fishing activity, especially for pelagic fisheries in the High Seas(Kerry et al., 2022). New reconstructions of fishing effort that include artisanal and industrial sectors provide more nuanced insights on the development of regional fisheries (Rousseau et al., 2019, 2024). Regional catch reconstructions have revealed the importance of "straddling" species, which forage both within exclusive economic zones and in the High Seas over the course of a year, thus disconnecting regions of fish biomass production from regions of biomass extraction (Sumaila et al., 2015). Analysis of catch data shows how energy inputs at the base of food webs determine the dominance of pelagic vs. demersal communities across latitudes (van Denderen et al., 2018), suggesting different temperature sensitivities of growth for these groups (van Denderen et al., 2020). Finally, harmonization and in-depth analysis of fisheries-

https://doi.org/10.5194/gmd-2024-26
Preprint. Discussion started: 2 May 2024


Geoscientific Model Development Discussions

independent trawl data has begun to reveal large-scale fish biomass patterns with unprecedented accuracy (Maureaud et al., 2023).

Here, motivated by discrepancies between observations and simulations with the original BOATS model (BOATSv1) and insights from recent large-scale studies, we revise the model formulation to improve its representation of High Sea vs. coastal fisheries, and of pelagic vs. demersal communities, leading to a significant model update: BOATSv2. The rest of the paper consists of four main Sections. Section 2 summarizes the main principles of BOATSv1. Section 3 details previous model developments and new features introduced in BOATSv2. Section 4 describes a revised model optimization procedure, leading to 5 optimal parameter ensembles. Section 5 compares the old and new model versions, showing how BOATSv2 improves the representation of global fisheries, and discussing insights from the new formulation.

2 BOATSv1

The philosophy of BOATS is to ensure global applicability while including sufficient ecological and economic complexity to represent realistic first-order fishery dynamics. The model is designed with a relatively small number of parameters, facilitating objective parameter optimization. It can simulate marine ecosystems on a 2-dimensional spatial grid, from small regions to the global ocean. In the following, we provide a brief overview of key model principles, and refer the interested reader to Appendix A for all equations and to previous publications for detailed explanations (Carozza et al., 2016, 2017).

2.1 Ecological module

BOATSv1 simulates the biomass of commercial fish by size, f_k (in $\mathrm{g\ m^{-2}\ g^{-1}}$, where g are grams of wet biomass), and its propagation across a spectrum of size classes $[m_0, m_u]$, where m is the biomass of an individual fish (in g). Here, different fish groups are indicated with the subscript k, with n_k groups distinguished by their asymptotic mass $m_{\infty,k} < m_u$. The total biomass density $B_k = \int_{m_0}^{m_{\infty,k}} f_k \, dm$ is the sum of all biomass across individual size classes (in $\mathrm{g\ m^{-2}}$). The propagation of biomass through the size spectrum of each group as a function of time t is described by the McKendrick von Foerster equation, with appropriate boundary and initial conditions:

$$\begin{cases} \dfrac{\partial}{\partial t} f_k = -\dfrac{\partial}{\partial m} \gamma_{S,k} f_k + \dfrac{\gamma_{S,k} f_k}{m} - \Lambda_k f_k - h_k \\ \gamma_{S,k} f_k = R_{P,k} \dfrac{R_{e,k}}{R_{P,k} + R_{e,k}} \text{ for } m = m_0 \\ f_k = f_{k,m,0} \text{ at } t = 0 \end{cases} \tag{1}$$

with $R_{e,k}$ and $R_{P,k}$ that are respectively the biomass input potential at recruitment size m_0 from eggs production e, and the primary production input to juveniles (in $\mathrm{g\ m^{-2}\ s^{-1}}$), $\gamma_{S,k}$ a size-dependent growth rate (in $\mathrm{g\ s^{-1}}$), and Λ_k a natural mortality rate (in $\mathrm{s^{-1}}$). The sink term h_k (in $\mathrm{g\ m^{-2}\ g^{-1}\ s^{-1}}$) is the biomass harvest by fishing that couples the ecological module to the fisheries dynamics module (see Section 2.2). The initial biomass distribution $f_{k,m,0}$ approximates an ocean in the absence of fishing ("pristine"), and is estimated from environmental conditions (Section 3.3).

https://doi.org/10.5194/gmd-2024-26
Preprint. Discussion started: 2 May 2024

Geoscientific Model Development Discussions

The growth rate, for a given fish size, is proportional to the minimum between the energy provided by primary production to that size, given trophic transfer across the food-web $\xi_{P,k}$, and the production potential for that size following individual-level allometric growth $\xi_{VB,k}$ (in g s^{-1}):

$$\gamma_{S,k} = (1-\Phi_k)\,\xi_{I,k} = (1-\Phi_k)\,min\left(\xi_{P,k}, \xi_{VB,k}\right) = min\left(\frac{\phi_{C,k}\pi m}{f_k}, Am^b - k_a m\right) \quad (2)$$

for $(1-\Phi_k)$ the remainder of energy allocated to growth when a fraction Φ_k is allocated to reproduction (see Appendix A for more detail). Thus, when food is limiting, individual fish will grow according to $\pi = \Pi_\psi / m_\psi (m/m_\psi)^{\tau-1}$, which defines a spectrum of available energy from primary production as a function of size (in g m^{-2} g^{-1} s^{-1}). Here, τ is the trophic scaling, and m_ψ a representative cell size for primary producers (i.e., phytoplankton) at the base of the food-web Π_ψ (in mmol C m^{-2} s^{-1}). These two parameters determine the efficiency of propagation of production through the consumer size spectrum, and the length of the food-web leading to higher trophic levels. Primary production is equally partitioned across the groups, i.e., $\phi_{C,k} = 1/n_k$. When food is in excess of what can be consumed by the standing fish biomass, fish grow as fast as physiologically possible, given an allometric scaling b, a temperature dependent anabolism $Am^b = A_0\ a_A(T) m^b$ and catabolism $k_a m = A\epsilon_a\ m_{\infty,k}^{b-1} m$, where A_0 is a growth constant (in g s^{-1}), and ϵ_a an activity fraction. The temperature dependence $a_A(T)$ follows a van't Hoff-Arrhenius curve controlled by a growth activation energy $\omega_{a,A}$ (in eV).

Recruitment provides the boundary condition, setting the flux of biomass at the lower mass boundary m_0. Recruitment is a function of the biomass production by mature individuals $R_{e,k} = F(\gamma_{R,k})$ assuming that a fraction Φ_k of the input energy is allocated to reproduction, $\gamma_{R,k} = \Phi_k \xi_{I,k}$. The recruitment flux is determined by summing all individual contributions across sizes m for a fraction of females ϕ_f and an egg survival probability s_e. Primary production limits the survival of recruits, saturating toward the limit $R_{P,k} = \phi_{C,k}\pi(m_0)m_0$, which is controlled by the energy available from primary production at the recruit size m_0. In high-biomass regions with large egg production, recruitment is thus generally constrained by $\pi(m_0)$.

The natural mortality rate (in units of s^{-1}) depends on both individual and asymptotic mass, following:

$$\Lambda_k = e^{\zeta_1} \frac{A_0}{3} a_\lambda(T) m^{-h} m_{\infty,k}^{h+b-1} \quad (3)$$

where h is an allometric scaling, and ζ_1 (in g s^{-1}) a mortality rate parameter. To account for separate temperature dependencies between metabolism $a_A(T)$ and other processes such as predator-prey interactions, mortality varies with a distinct temperature dependence $a_\lambda(T)$, following a van't Hoff-Arrhenius curve set by an activation energy $\omega_{a,\lambda}$ (in eV).

For this ecological module Eqs. (1-3), 9 parameters are not well constrained by the literature (see Table 1): the activation energies $\omega_{a,A-\lambda}$; the scaling exponents b and h; the constants A_0 and ζ_1; the trophic scaling $\tau = log(\alpha)/log(\beta)$, itself a function of trophic efficiency α and predator-prey mass ratio β; and the egg survival fraction s_e. In previous work (Carozza et al., 2017), these parameters are selected from prior ranges by applying a Monte Carlo approach, keeping a small ensemble of 5 parameter sets to account for parameter uncertainty (see Section 4.2). Compared to the calibration of BOATSv1 (Carozza et al., 2017), we assume that a subset of parameters (k_E and Π^*) are relatively well constrained, since previous analysis have shown that their variation had no significant effect. For this update, we replicate the Monte Carlo selection procedure, after updating a few prior parameter ranges based on recent analyses (α (Stock et al., 2017; Eddy et al., 2020)) and because previously optimized values were close to the boundaries of the ranges (b, s_e).

https://doi.org/10.5194/gmd-2024-26
Preprint. Discussion started: 2 May 2024

Geoscientific Model Development Discussions

For a given set of parameters, the dynamics of commercial fish biomass in BOATSv1 is determined by two spatially and temporally varying environmental "forcings": local primary production Π_ψ and epipelagic temperature $T = T_{75}$ (average temperature in the top 75m).

2.2 Economic module

BOATSv1 couples fish biomass and fishing effort E_k (in $\mathrm{W\ m^{-2}}$) to determine fish catch rate C_k (in $\mathrm{g\ m^{-2}\ s^{-1}}$) for each group k. Fishing effort is typically initialized everywhere at zero and evolves independently in each grid cell under an open-access dynamic, proportional to the local net profit (the difference between revenue and cost) as:

$$\begin{cases} \dfrac{d}{dt}E_k = \kappa_e \dfrac{revenue_k - cost_k}{E_k} \\ E_k = 0 \text{ at } t = 0 \end{cases} \tag{4}$$

where κ_e (in $\mathrm{W^2\ m^{-2}\ \$^{-1}}$) is a fleet dynamic parameter that sets the effort adjustment timescale for a given change in profit.

The rate of revenue obtained over a time interval dt at some point in the ocean (in $\mathrm{\$\ m^{-2}\ s^{-1}}$) is determined as a spectrum r_k (in $\mathrm{\$\ m^{-2}\ s^{-1}\ g^{-1}}$) that is defined separately for each group f_k. It represents the product of catch and the mass-specific price fishers are paid at port, integrated across size classes within each group:

$$revenue_k = \int_{m_0}^{m_{\infty,k}} r_k dm\ dt\ = p_k q_k E_k dt \int_{m_0}^{m_{\infty,k}} \sigma_k f_k dm \tag{5}$$

where p_k is the selling price (in $\mathrm{\$\ g^{-1}}$) of the group, $\sigma_k f_k$ is the biomass targeted by fishing, and σ_k is a size-dependent selectivity of fishing gear on group k. The selectivity plays a fundamental role by distributing fishing effort across size classes. Here, it is defined as a sigmoidal curve that applies reduced effort to the smallest sizes, approximating the selectivity of towed gear such as trawls and seines. The parameter $e_{m_{\Theta,k}}$ accounts for the uncertainty around a target threshold mass $m_{\Theta,k} = d_{m_{\Theta,k}} e_{m_{\Theta,k}} m_{\alpha,k}$, which is proportional to the maturity mass for each group $m_{\alpha,k}$. Specifically, $d_{m_{\Theta,k}}$ is set to select mainly mature individuals (i.e., $d_{m_{\Theta,k}} = 1$) such that $e_{m_{\Theta,k}}$ reflects a variability around this mass. The catchability q_k (in $\mathrm{m^2\ W^{-1}\ s^{-1}}$) per unit of nominal fishing effort encapsulates the ability of fishing effort to extract fish biomass, reflecting the inherent characteristics of the fish group as well as the fishing technology (including gear, navigation instruments, sonars, and communication) and accrued knowledge (Palomares and Pauly, 2019).

Net profits are determined by subtracting costs from revenues. Similar to revenue, the cost is expressed as the average expenditure rate per time over an area of the ocean (in $\mathrm{\$\ m^{-2}\ s^{-1}}$). In reality, the cost of fishing includes the purchase and maintenance of capital, fuel costs for transit between fishing grounds and ports as well as during gear operation, and labour. In the model, cost is simply proportional to effort, $cost_k = c_k E_k dt$, where c_k is the cost per unit effort ($\mathrm{\$\ W^{-1}\ s^{-1}}$). When revenue exceeds costs, fishing effort Eq. (4) increases. Any nonzero effort will lead to fish catch:

$$h_k\ dt\ dm = q_k \sigma_k\ E_k\ f_k\ dt\ dm \tag{6}$$

https://doi.org/10.5194/gmd-2024-26
Preprint. Discussion started: 2 May 2024

Geoscientific Model Development Discussions

Table 1. Model parameters and summary results for the Monte Carlo ensemble (update of Table 3 in Carozza et al. (2017)). The sampling distribution of each parameter used in the Monte Carlo simulation are shown, where $X(p1, p2)$ represents the probability distribution (N for normal, U for uniform), and $p1$ and $p2$ are the mean and standard deviation of each parameter, respectively, for the pelagic P and demersal D communities when it applies. Opt. refers to the subset of optimized Monte Carlo simulations, N.O. to the subset of non-optimized simulations. SD is the standard deviation, and KS p-value is the p-value of the 2-sample Kolmogorov-Smirnov test applied to the optimized and non-optimized sets. The three last variables are fixed compared to previous optimizations.

Parameter	Name	Sampling Distribution	Mean Opt.	Mean N.O.	SD Opt.	SD N.O.	KS-pvalue
$\omega_{a,A}$	Growth activation energy	$U_P(0.45, 0.09)$	0.50	0.45	0.088	0.089	$4.7\ 10^{-3}$
		$U_D(< U_P, 0.09)$	0.37	0.30	0.14	0.13	$2.6\ 10^{-3}$
$\omega_{a,\lambda}$	Mortality activation energy	$U_P(0.45, 0.09)$	0.45	0.45	0.079	0.090	0.59
		$U_D(0.45, 0.09)$	0.45	0.45	0.096	0.090	0.57
b	Allometric scaling exponent	$N(0.55, 0.12)$ & $N(0.70, 0.12)$*	0.72	0.63	0.06	0.15	$1.4\ 10^{-9}$
A_0	Allometric growth constant	$N(4.46, 0.50)$	4.7	4.46	0.47	0.50	0.053
h	Allometric mortality scaling	$N(0.54, 0.09)$	0.51	0.54	0.064	0.089	$1.1\ 10^{-3}$
ζ_1	Mortality constant	$N(0.55, 0.57)$	-0.072	0.54	0.38	0.57	$3.6\ 10^{-10}$
α	Trophic efficiency	$U(0.23, 0.10)$	0.14	0.23	0.027	0.098	$6.9\ 10^{-14}$
β	Predator to prey mass ratio	$U(5000, 2500)$	4970	5000	2580	2510	0.94
τ	Trophic scaling	$log(\alpha)/log(\beta)$	-0.24	-0.19	0.016	0.063	$3.5\ 10^{-17}$
s_e	Egg survival fraction	$U(0.05, 0.028)$	0.052	0.050	0.025	0.028	0.49
$e_{m_{\Theta,k}}$	Selectivity position scaling	$U(0.75, 0.2)$	0.77	0.75	0.20	0.20	0.54
$log_{10}(m_\beta)$	Mean benthic size	$N(-6.5, 0.67)$	-6.4	-6.51	0.47	0.67	0.064
k_E	Eppley constant	-	0.06	-	-	-	-
Π^*	Nutrient concentration	-	0.35	-	-	-	-
c_σ	Selectivity slope	-	17.8	-	-	-	-

*We merge 2 ensembles of 10000 simulations each, with slightly different distributions for b. The first ensemble prompted re-selection of the parameter range for the second.

which couples the economic and biological modules Eq. (1). A catch limit is imposed for numerical stability (i.e., to prevent harvesting more fish than the available biomass). The total catch rate for each group is then given by: $C_k = \int_{m_0}^{m_{\infty,k}} h_k dm$ (in g m^{-2} s^{-1}.

In the open-access economic model, only a single parameter, $e_{m_{\Theta,k}}$ (the threshold mass for fishing selectivity), remains undetermined and is included in the Monte Carlo analysis. Compared to previous implementations, we fixed the selectivity slope parameter c_σ for all simulations since previous analysis showed limited sensitivity; the range was also updated to reflect a selectivity around maturation size (Carozza et al., 2017).

In BOATSv1, the ex-vessel fish price p_k is generally assumed to be constant in space and time, since observations suggest small historical variations (Sumaila et al., 2007; Galbraith et al., 2017). Similarly, cost c_k is also assumed constant. Catchability q_k increases annually at a 5% rate that accounts for sustained technological improvements and is the only temporally-varying economic "forcing".

https://doi.org/10.5194/gmd-2024-26
Preprint. Discussion started: 2 May 2024

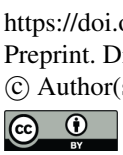

Geoscientific Model Development Discussions

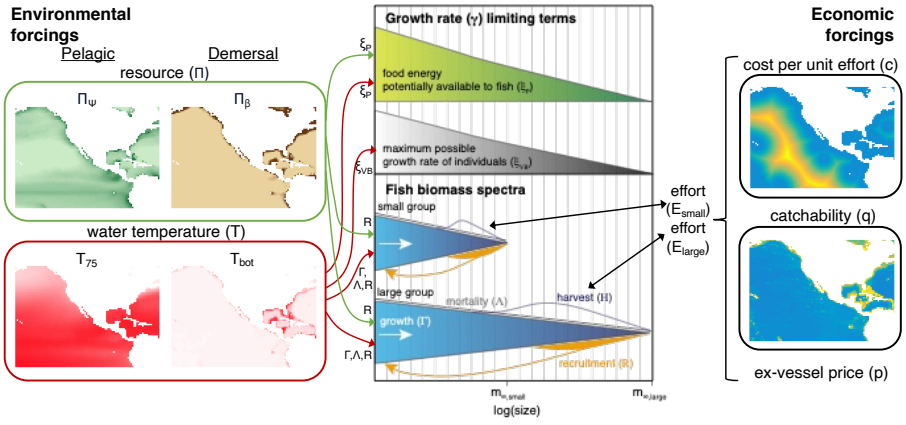

Figure 1. Schematic diagram of the main modules, components, and processes of BOATSv2. Updated from the schematic diagram in Carozza et al. (2017).

3 BOATSv2

Here we describe the features of BOATSv2 that provide an update to the original BOATSv1. Two of these features were introduced incrementally, in previously-published work, in order to capture iron limitation in regions where iron is known to be scarce (Galbraith et al., 2019), and to represent management of fisheries (Scherrer and Galbraith, 2020; Scherrer et al., 2020). Below we provide a brief summary of these previous updates, before discussing in detail the novel features. A schematic of BOATSv2 is provided in Figure 1.

3.1 Previously-published features

3.1.1 Reduced growth rates in iron-limited regions

Iron limitation of phytoplankton growth is widely recognized in the ocean, most prominently in HNLC regions (Tagliabue et al., 2017). Less is known about iron limitation of higher trophic levels in the ocean, including fish (Le Mézo and Galbraith, 2021). Multiple lines of evidence suggest that low iron availability also places strong limits on fish growth, and could contribute to reducing fish abundance in large portions of the High Seas (Galbraith et al., 2019).

Following Galbraith et al. (2019), we simulate iron limitation of fish by modulating the trophic efficiency α, which determines the fraction of biomass incorporated into new tissues at each trophic step, with the following function:

$$\alpha^{corr} = \alpha \left(\frac{k_{NO_3^-}}{k_{NO_3^-} + NO_3^-} \right) \tag{7}$$

where the surface concentration of nitrate (NO_3^-, in µM) is taken as a proxy for iron limitation, in the absence of reliable globally resolved estimates of surface iron concentrations or plankton iron contents. This formulation smoothly decreases the trophic efficiency as surface nitrate increases. The constant $k_{NO_3^-} = 5$ µM controls the strength of this effect, and is constrained

https://doi.org/10.5194/gmd-2024-26
Preprint. Discussion started: 2 May 2024


Geoscientific Model Development Discussions

empirically. Nitrate concentrations are taken as the monthly minimum from the World Ocean Atlas (WOA) climatology (Locarnini et al., 2006) (see Appendix B). Although uncertainties persist regarding the impact of iron limitation on marine predators, this parameterization effectively reduces an overestimate in fishing effort in the Southern Ocean, North Pacific, and North Atlantic in BOATSv1 (Galbraith et al., 2019).

3.1.2 Management with varying effectiveness

In BOATSv1, effort was generally assumed to follow an open-access dynamic Eq. (4). This was modified to represent the influence of regulation by adjusting fishing effort to align with a prescibed target $E_{targ,k}$ (Scherrer and Galbraith, 2020), as:

$$\left(\frac{d}{dt}E_k\right)^{corr} = \left(\frac{d}{dt}E_k\right)e^{-S} + \left(1-e^{-S}\right)\kappa_s\left(E_{targ,k} - E_k\right) \tag{8}$$

where S is a non-dimensional parameter representing how effectively the target is enforced. When $S = 0$ the model follows open-access dynamics; when $S > 0$ the nominal effort is nudged towards the target at a rate proportional to the regulation response parameter κ_s ($\mathrm{m}^{-2}\ \$^{-1}$).

This feature showed that strong fisheries regulation is required to prevent overfishing if technological progress keeps increasing, making management effectiveness a key factor in future scenarios (Scherrer and Galbraith, 2020). For the rest of the paper, we set $S = 0$, and focus on simulation of historical fisheries up to the time they reached maximum catches, for which the open-access dynamic was shown to be adequate (Galbraith et al., 2017; Guiet et al., 2020).

3.2 Novel model features

3.2.1 Separate pelagic and demersal energy pathways

Variations in energy input at the base of marine food webs significantly affect biomass accumulation and cycling, thereby altering the sensitivity of different fish communities to climate and environmental factors (Petrik et al., 2019). Pelagic communities are more tightly tied to surface planktonic production (i.e., net primary production Π_ψ), whereas benthic communities depend on the delivery of organic material the seafloor (i.e., particle flux at bottom Π_β in $\mathrm{mmol\ C\ m^{-2}\ s^{-1}}$) (Stock et al., 2017; van Denderen et al., 2018). The two types of communities also experience different temperatures, with surface temperature (here, $T = T_{75}$) controlling the metabolic rates of pelagic fish, and bottom temperature ($T = T_{bot}$) that of demersal fish.

To account for these ecological differences, we modified BOATS to resolve separate pelagic and demersal fish communities. Both communities are described by the same set of equations, solved independently (see environmental forcing Fig. 1). Pelagic fish are forced by surface conditions (Π_ψ and $T = T_{75}$), while demersal fish are forced by bottom conditions (Π_β and $T = T_{bot}$). Whereas the energy supply to the pelagic community remains dependent on surface NPP, the particle flux to the bottom provides the energy input to the demersal community. The particle flux is modeled as a depth-dependent fraction of surface primary production:

$$\Pi_\beta = \Pi_\psi * pe_{ratio} * \left(\frac{z_{bot}}{z_{eu}}\right)^{b_a}. \tag{9}$$

https://doi.org/10.5194/gmd-2024-26
Preprint. Discussion started: 2 May 2024

Geoscientific Model Development Discussions

This formulation assumes a power-law decrease of the flux of organic material below the euphotic layer, i.e., a typical Martin curve (Martin et al., 1987; Buesseler and Boyd, 2009). The attenuation coefficient $b_a = -0.8$ and the euphotic layer depth $z_{eu} = 75$ m are assumed to be fixed, although they could be modeled to vary with space and time. Here, similar to prior work (Stock et al., 2017; van Denderen et al., 2018; Petrik et al., 2019), we focus on first-order variations in fish biomass in increasingly deep habitats, where food becomes progressively scarce. We calculate the term $(z_{bot}/z_{eu})^{b_a}$ using the high-resolution bathymetry z'_{bot} from the ETOPO global surface relief at $1/10^o$th (Amante and Eakins, 2009), and taking the average across 1^o grid cells $(z_{bot}/z_{eu})^{b_a} = \overline{(z'_{bot}/z_{eu})^{b_a}}$. Note that, when z'_{bot} is shallower than z_{eu}, export is only determined by the pe_{ratio}, which is taken as a function of surface temperature T_{75} and net primary production Π_ψ, following Dunne et al. (2005).

In the pelagic ocean, the typical size of phytoplankton, m_ψ, varies markedly between productive and oligotrophic regions. This variation affects both the length of the food web and the proportion of production accessible to fish communities (Ryther, 1969). In analogy with the pelagic ecosystem, we assume that the representative size of benthic organisms at the base of the demersal food-web, m_β, influences the fraction of energy that reaches demersal fish. For simplicity, we take m_β to be globally uniform. Unlike m_ψ, for which empirical parameterizations exist, m_β is poorly constrained, and is included in the Monte Carlo optimization procedure (Table 1), with a prior range of values $[10^{-8}, 10^{-5}]$ g. We keep most food-web parameters the same for pelagic and demersal fish, with the exception of the activation energy $\omega_{a,A-\lambda}$, since observations suggest significant differences between the two communities (van Denderen et al., 2020).

3.2.2 Heterogeneous costs

Simulations with BOATSv1 suggest that variations in the cost per unit effort of fishing c_k (in \$ $\mathrm{W}^{-1}\,\mathrm{y}^{-1}$) played only a secondary role in the development of global fisheries (Galbraith et al., 2017). Yet, heterogeneous costs in the global ocean could modulate the spatial distribution of fishing effort and its evolution over time (Swartz et al., 2010; Anticamara et al., 2011; Lam et al., 2011). Reconstructions of fishing effort in the High Seas suggest more than twofold average cost differences between distinct fishing gears and regions (see Sala et al. (2018); Kroodsma et al. (2018) and Appendix C).

To simulate the effect of heterogeneous fishing costs on the historical offshore expansion of fisheries, we replaced the constant costs per unit effort ($c_k = 5.85$ \$ $\mathrm{W}^{-1}\,\mathrm{y}^{-1}$) in BOATSv1 by spatially-varying costs, using a linear function of the distance to shore for effort targeting pelagic fish, d_{coast} (in km), and a linear function of seafloor depth z_{bot} (in m) for effort targeting demersal fish (see economic forcing Fig. 1):

$$c_k^{corr}\,(x = d_{coast}, z_{bot}) = \begin{cases} c_k \;\; \text{when} \;\; x \leq x^* \\ c_k + \delta(x - x^*) \;\; \text{when} \;\; x > x^* \end{cases} \tag{10}$$

where x^* is a reference parameter that determines the boundary between coastal and High Seas regions. For pelagic effort, x^* identifies a coastal band over which transit costs are assumed to be small compared to other costs. Here we adopt $x^* = 370$ km. For demersal effort, x^* identifies a depth threshold above which the cost of setting and hauling gears is negligible compared to other costs, and set $x^* = 200$ m. The parameter δ is the proportionality constant for the increase of costs beyond these coastal bands (in \$ $\mathrm{km}^{-1}\,\mathrm{W}^{-1}\,\mathrm{y}^{-1}$ for pelagic effort, and \$ $\mathrm{m}^{-1}\,\mathrm{W}^{-1}\,\mathrm{y}^{-1}$ for demersal effort).

https://doi.org/10.5194/gmd-2024-26
Preprint. Discussion started: 2 May 2024

Geoscientific Model Development Discussions

For distance-dependent costs, we select $\delta = 7.9\ 10^{-3}$ \$ km^{-1} W^{-1} y^{-1}, such that the average High Seas fishing cost is 9.3 \$ W^{-1} y^{-1}, comparable with an empirical upper mean value of 8.9 \$ $\mathrm{W}^{-1}\mathrm{y}^{-1}$ (see Appendix C). For depth-dependent costs, the depth of the fishing grounds z_{bot} is determined from high resolution ($1/10^o$th) bottom topography (Amante and Eakins, 2009), taking the shallowest depth in each 1^o model grid cell. We set $\delta = 2.5\ 10^{-3}$ \$ m^{-1} W^{-1} y^{-1}, such that the average High Seas fishing cost is 9.9 \$ W^{-1} y^{-1} for exploitation of deep demersal stocks, comparable with an empirical upper boundary of mean High Seas trawling costs of 9.2 \$ W^{-1} y^{-1} (Appendix C). We tested distance and depth dependent costs both separately and combined to determine the impact on the model results.

3.2.3 Heterogeneous catchability

In BOATSv1, technological progress, represented by an exponential increase in the catchability q_k at a rate of 5% y^{-1}, was shown to be a dominant driver of the development of fisheries (Galbraith et al., 2017). While a homogeneous increase rate approximates the first-order effect of technological progress well, heterogeneous technological efficiencies among fisheries could modulate this development across regions (Palomares and Pauly, 2019), especially as separate gears target distinct resources and are deployed in different ecosystems (Kroodsma et al., 2018). Similar to cost, spatially-heterogeneous catchability could have influenced the spatial expansion of fisheries and or the deepening of catches with time (Watson and Morato, 2013).

To simulate the effect of heterogeneous catchability, the exponential increase is spatially weighted (see economic forcing Fig. 1):

$$q_k^{corr}\,(x = z_{bot}, y = P \text{ or } D) = q_k\ Pr(x)\ Of(y) \tag{11}$$

where $Pr(x = z_{bot})$ accounts for spatial variations of technological efficiencies with seafloor depth, and $Of(y = P \text{ or } D)$ offsets between the catchability of pelagic vs. demersal resources.

Commercially exploited fish often aggregate near seamounts and other shallow features, resulting in the local establishment of fisheries (e.g. 57% of longlining activity, Kerry et al. (2022)). The coarse resolution of BOATS prevents a direct representation of seamounts. However, the presence of seamounts could increase both fish biomass density and profitability within a model's grid cell, as opposed to the case where resources were more homogeneously distributed across the grid cell. The profile $Pr(x = z_{bot})$ parameterizes the effect of seamounts, and more generally an increase in the density of resources in shallow regions:

$$Pr(x = z_{bot}) = q_{min} + (1 - q_{min})\frac{log_{10}(x_{max}) - log_{10}(x)}{log_{10}(x_{max}) - log_{10}(x_{mean})} \tag{12}$$

Here, $q_{min} = 0.8$ is the minimum efficiency of gears targeting pelagic resources (see Appendix D), and x_{mean} and x_{max} respectively 2372 and 5750 m depth, based on the median and deepest depths of seamounts where fishing activity occurs (Kerry et al., 2022). The depth of the fishing grounds z_{bot} is determined from ETOPO at $1/10$th resolution (Amante and Eakins, 2009), coarsened by taking the shallowest depth in each 1^o model grid cell, as described above.

The dominant gears used to target different communities (pelagic vs. demersal) are characterized by different efficiencies (see Appendix D). We tested the effect of separate catchabilities for pelagic and demersal communities, setting $Of(P) =$

https://doi.org/10.5194/gmd-2024-26
Preprint. Discussion started: 2 May 2024


Geoscientific Model Development Discussions

$1.4\,Of(D)$. This offset was estimated from the technology coefficients of different gear targeting pelagic and demersal species, weighted by the fraction of global fishing effort for 16 different gears (Kroodsma et al., 2018; Palomares and Pauly, 2019).

3.3 Forcing and initialization

Forcing BOATSv2 requires surface temperature T_{75}, bottom temperature T_{bot} and net primary production Π_ψ. Since we are interested in the recent ocean state, we use climatological observations, and, to assess improvements between BOATS versions, we adopt the same forcing as in Carozza et al. (2017). Surface temperature (T_{75}) and temperature at the seafloor (T_{bot}) are taken from the World Ocean Atlas 2009 (Locarnini et al., 2006). T_{75} is calculated as the mean temperature over the top 75 m on a 1^o grid. T_{bot} is calculated by averaging temperatures at different depths, weighted by the fraction of each depth within a model grid cell as reported by the ETOPO $1/10$ bathymetry dataset (Amante and Eakins, 2009). For Π_ψ we take the average of three satellite-based estimates at 1^o resolution (Behrenfeld and Falkowski, 1997; Carr et al., 2006; Marra et al., 2007). Note that Π_ψ, and then Π_β, are forced once converted to $\mathrm{g\ m^{-2}\ s^{-1}}$.

The model is initialized by a "pristine" ocean biomass distribution determined by spinning-up the model without fishing for 300 years to reach a steady state. Then, the ecological and economic modules are run together with an increase of the catchability q_k for another 300 years. In a given region, fishing begins once catches becomes profitable (i.e., $revenue_k > cost_k$ in Equation 4). The open-access dynamics generally drives first an increase in catch, followed by a peak and decline due to overfishing (Guiet et al., 2020). To align simulations with observation (see Section 4.1), we estimate the time of the peak catch integrated across LMEs, and align it with the time of the observed peak catch, which occurs in the 1990s (Pauly and Zeller, 2016).

4 Parameterization and sensitivity

In this Section, we first describe the observation used for the evaluation of BOATSv2, and then detail the procedure used to parameterize the model, which is based on the following two steps (Fig. 2). (1) Ecological update: in coastal seas where economic parameterizations are more homogeneous, we parameterize separate pelagic and demersal pathways (Π_ψ & Π_β) and growth limitation in HNLC regions for pelagic species (α^{corr}), to determine the best parameter sets for the 11 undetermined parameters of the ecological module (see Table 1). (2) Economic update: we then fine-tune the parameters of the economic module using spatially heterogeneous costs and catchability in the global ocean (i.e., c_k^{corr} & q_k^{corr}).

4.1 Observational data and diagnostics for model evaluation

We use multiple empirical data sources, including catch, biomass and fishing effort, to tune and evaluate BOATSv2. Comparisons are made on globally integrated quantities, quantities integrated across LMEs to assess regional variability in coastal regions, and quantities integrated beyond the boundary of LMEs, across High Seas Ecosystems (HSEs, see Appendix E) to assess variability in the open ocean away from coastal influences. We focus on observations around the peak catch in the 1990s, but also include observations in the 1950s and 2000s for additional insight.

https://doi.org/10.5194/gmd-2024-26
Preprint. Discussion started: 2 May 2024

Geoscientific Model Development Discussions
Open Access
EGU

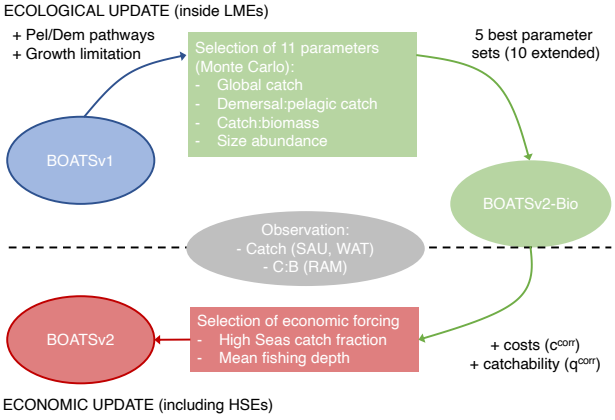

Figure 2. Schematic diagram of the parameterization procedure starting from BOATSv1 (in blue), with two steps: (1) Ecological update (in green), and (2) Economic update (in red). Observation used for parameterization of both are shown in gray steps.

For fish catch, we use two catch reconstruction datasets: (1) The Sea Around Us project (Pauly et al. (2020), SAU), corrected for under-reported catch. For the SAU, catches by functional type allow to separate pelagic (P) and demersal (D) species (see Appendix F). (2) The database from Watson (2017) (hereafter WAT), including wild catch and corrected for illegal and unreported fisheries. When comparing catches by LME, we focus on 55 LME (out of 66) and ignore the Black Sea and a number of high-latitude regions to avoid errors caused by biases in satellite-based chlorophyll and the lack of representation of the effects of sea ice on the marine ecosystem (as in Carozza et al. (2017)). We define two diagnostics to help correct for biases in BOATSv1: the fraction of catch in the High Seas, $R_C = C_{HS}/(C_{HS} + C_{CS})$, and the catch-weighted mean depth of fishing $Z_C = (\sum_{lat,lon} C z_{bot})/(\sum_{lat,lon} C)$ (in m).

For biomass observations, we use the RAM Legacy stock assessment database (Ricard et al., 2012). Stock assessment data are used to estimate mean catch to biomass ratios (C:B hereafter) in 25 LMEs where enough stock assessments are available, following Bianchi et al. (2021). We also compare historical changes in fish biomass to a global reconstruction based on stock assessments (Worm and Branch, 2012). Furthermore, we compare the model with two biomass databases derived from fisheries-independent surveys: the first, encompassing demersal species across 14 Large Marine Ecosystems (LMEs) in the Northern Hemisphere, ranging from the Bering Sea to Northern Europe, is based on a recent synthesis of bottom trawl data (van Denderen et al., 2023; Maureaud et al., 2023). The second, focusing on pelagic species, is built on standardized trawls of coastal pelagic species in 2 LMEs along the North American West Coast (Zwolinski et al., 2012).

Finally, we include a comparison with reconstructions of nominal effort for the global fishing fleet in both artisanal and industrial sectors, to shed light on the regional development of fisheries (Rousseau et al., 2019, 2024). Similar to catch, we focus on a subset of 55 LMEs where model forcings are more suitable.

https://doi.org/10.5194/gmd-2024-26
Preprint. Discussion started: 2 May 2024

Geoscientific Model Development Discussions
Open Access
EGU

4.2 Ecological update: Monte Carlo ensemble

To calibrate the revised model and specify the value of 11 poorly determined parameters (Table 1), we adopt an ensemble Monte Carlo approach, following previous work (Carozza et al., 2017; Bianchi et al., 2021). These parameters impact size-dependent growth (b, A_0, α and β), size dependent mortality (h ζ_1), and the effect of temperature ($\omega_{a,A/\lambda}$). They also impact recruitment (s_e), and the biomass transfer towards demersal consumers (m_β). Finally they affect the selectivity of fishing gear ($e_{m_{\Theta,k}}$). We keep the same parameters for both pelagic and demersal communities, except for the temperature dependence.

We run $20,000$ simulations, each with a distinct combination of parameters, integrated with gradually increasing catchability over time, and select the best simulations according to global and local criteria. These criteria are updated from Carozza et al. (2017) to provide an evaluation of the model performance in reproducing the following features of pelagic and demersal communities:

- (1) Global catch. Simulations predict a global fish catch in line with observations, when integrated over the 55 LMEs, for the years of maximum catch in the 1990s, i.e., $C_{Globmax}^{SAU-WAT} \simeq 100 \times 10^6$ ton y^{-1} (using ton of wet biomass). There are significant uncertainties around these reconstructions; furthermore, migratory species not represented in BOATS can influence the model's maximum yields. Therefore, we allow catches to be within the range, $C_{Globmax} \in [70, 150] \times 10^6$ ton y^{-1}. We find that 12% of simulations in the Monte Carlo ensemble, which spans a total catch range of more than 6 orders of magnitude (see Fig. 3), satisfy this constraint.

- (2) Demersal:pelagic catch. At the global catch peak, pelagic and demersal catch integrated over all 55 LMEs account respectively for 45% and 55% of catches in SAU. That is, the ratio between demersal and pelagic catch at peak is $R_{Globmax,D/P}^{SAU} \simeq 1.2$. Because of uncertainties around the SAU reconstructions, the presence of migratory species, and additional uncertainty in the allocation of pelagic vs. demersal catch (Appendix F) we allow this ratio to vary within the range $R_{Globmax,D/P} \in [0.8, 1.8]$. In the Monte Carlo ensemble, this ratio varies by more than 3 orders of magnitude. However, we find that 20% of the simulations satisfy this condition, leaving us with 3.0% when combined with criteria 1 (Fig. 3).

- (3) Catch:biomass. To ensure that global catches are supported by realistic rates of fish biomass production, we compare the model catch to biomass ratio (C:B) averaged over 25 LMEs to the observational estimate from the RAM Legacy database (see Bianchi et al. (2021)). This is done by retaining simulations for which a Kolmogorov-Smirnoff test indicates that the modeled C:B ratios follow the same distribution as the stock assessment data, rejecting cases where distributions are found different at the 1% significance level. This condition leaves us with 0.8% of all simulations, when combined with criteria 1 and 2.

- (4) Size abundance. Finally, to preserve a realistic partitioning of fish catches by size groups, we constrain the catch of medium and large sizes to be in the observed range relative to fish in the small group, i.e., $0.3\ C_{small} < C_{med}$ and $0.1\ C_{small} < C_{lrg} < 0.8\ C_{small}$. Considering all four criteria, we are left with 42 simulations (0.2%).

https://doi.org/10.5194/gmd-2024-26
Preprint. Discussion started: 2 May 2024


Geoscientific Model Development Discussions

Criteria (1) to (4) identify parameter sets that best capture global properties of catches and properties of fish production per unit biomass, for both pelagic and demersal species, focusing on well-sampled coastal regions. The optimized parameters, compared to the non-optimized values, are reported in Table 1. Among these, 5 parameters (6 including the trophic scaling) differ significantly from the non-optimized prior distributions, based on a Kolmogorov-Smirnoff test (KS-pvalue<10^{-2}). These include the growth activation energy $\omega_{a,A}$, the allometric growth and mortality scaling exponents b, h, the mortality constant ζ_1, and the trophic efficiency α. The implications of these differences are discussed in Section 5.1.

Figure 4 shows the timeseries of catch, nominal effort, and biomass, over all 55 LMEs from 1900 to 2050 for the 42 simulations that meet all criteria. In each simulation, global catch increases until reaching a peak, beyond which biomass depletion limits recruitment and drives a fall in catch. Effort follows a comparable pattern, but with a consistent time lag. Biomass monotonically decreases from an initial, near pristine state. These features are comparable to observational reconstructions (Fig. 4a, C^{SAU} and C^{WAT}). A delayed response of nominal effort is also consistent with observations (Fig. 4b), while the consistent decrease in biomass compares well with aggregated stock assessment data normalized to the pristine period (Fig. 4c,d).

Similar to prior work with BOATSv1, we focus our analysis on 5 best ensemble members selected to capture parameter uncertainty, while maintaining reasonable computational costs. These 5 parameter sets are selected out of the 10 best of the 42 simulations, based on their ability to reproduce regional variability in peak catches by LMEs. The peak catch is determined almost exclusively by ecological parameters, making it a valuable way to discriminate amongst them (Carozza et al., 2017). Accordingly, we rank the 42 simulations by the Pearson correlation coefficient of simulated vs. observed catch in the 55 LMEs (r^{SAU}_{LMEmax}) and select 5 ensemble members out of the top 10. These 5 chosen parameter sets comprise diverse shapes of catch, effort and biomass histories, but, once averaged together, they provide an ensemble mean that matches the observed historical development of these quantities across LMEs ($r^{SAU}_{LMEmax} \in [0.63, 0.69]$, see Table 2 and Fig. 4, dark red lines). The 5 parameter sets span relatively wide ranges of values, thereby covering a broad range of uncertainty (see list in Table 2). The Pearson correlation coefficients r_{LME90s} between observed and simulated catch by LME at global peak are comparable with and without updated ecological features (see BOATSv1 compared to other model variants, Table 3, $r^{SAU}_{LME90s} \simeq 0.69$ and $r^{WAT}_{LME90s} \simeq 0.73$). However, the updated ecological features provide large improvements in the High Seas (e.g., r^{WAT}_{HSE90s} increases from 0.22 in v1 to 0.58).

4.3 Economic update: sensitivity to cost and catchability

As shown in Table 3, increased ecological realism improves the model's ability to reproduce High Seas fisheries, in particular the fraction of High Seas catch, R_C, and the catch-weighted mean depth of fishing, Z_C. These improvements reflect growth limitation in HNLC regions (α^{corr}) (Galbraith et al., 2019), and, to a greater extent, explicit separation of pelagic and demersal energy pathways (Π_ψ & Π_β+α^{corr}, hereafter BOATSv2-Bio, green line Fig. 5a,b).

Since economic drivers could explain additional spatial variability, we also incorporated heterogeneous costs (c_k^{corr}) and catchability (q_k^{corr}) in the simulations. Accordingly, we further evaluated the effect of considering different economic parameterizations, and selected the best combination based on global and regional criteria. This evaluation shows that:

https://doi.org/10.5194/gmd-2024-26
Preprint. Discussion started: 2 May 2024

Geoscientific Model Development
Discussions
Open Access
EGU

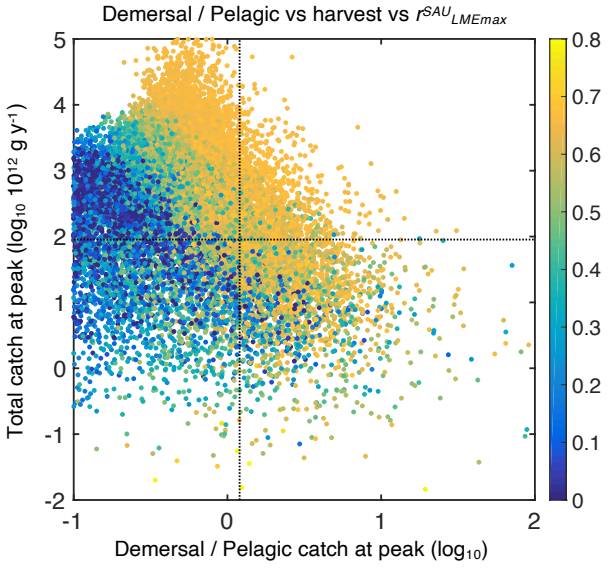

Figure 3. Simulations of global catch features from the BOATSv2 Monte Carlo ensemble. Total catch at global peak of the 1990s $C_{Globmax}$ is shown as a function of the ration between demersal and pelagic catch at the global catch peak, $R_{Globmax,D/P}$, for the $20,000$ simulations in the ensemble. Colors show the Pearson correlation coefficient r^{SAU}_{LMEmax} of simulated vs. observed (SAU) maximum catch in 55 LMEs C_{LMEmax}, for each simulation. The dotted horizontal line shows the reference global harvest, $C^{SAU-WAT}_{Globmax} = 100 \times 10^{12}$ g y^{-1}, and the dotted vertical line the observed ratio of demersal to pelagic catch at the global peak, $R^{SAU}_{Globmax,D/P} = 1.2$.

Table 2. List of parameter values for the selected 5 best simulations with updated ecological features.

	211	3773	14028	14349	15436
r^{SAU}_{LMEmax}	0.66	0.63	0.69	0.68	0.64
$\omega_{a,A}$	0.30/0.16	0.42/0.33	0.42/0.17	0.43/0.12	0.47/0.25
$\omega_{a,\lambda}$	0.53/0.61	0.47/0.49	0.39/0.61	0.43/0.57	0.42/0.51
b	0.73	0.75	0.75	0.80	0.70
A_0	4.35	4.49	4.35	5.04	4.49
h	0.49	0.55	0.46	0.46	0.55
ζ_1	-0.10	-0.68	-0.07	-0.25	-0.33
α	0.14	0.09	0.10	0.12	0.12
β	2830	5890	8890	8510	6330
τ	-0.24	-0.27	-0.25	-0.23	-0.24
$e_{m_{\Theta,k}}$	0.44	0.76	0.97	0.75	0.67
s_e	$9.3\ 10^{-2}$	$5.0\ 10^{-2}$	$4.8\ 10^{-2}$	$2.7\ 10^{-2}$	$2.4\ 10^{-2}$
$log_{10}(m_\beta)$	-6.6	-6.0	-6.1	-6.6	-6.0

https://doi.org/10.5194/gmd-2024-26
Preprint. Discussion started: 2 May 2024

Geoscientific Model Development Discussions

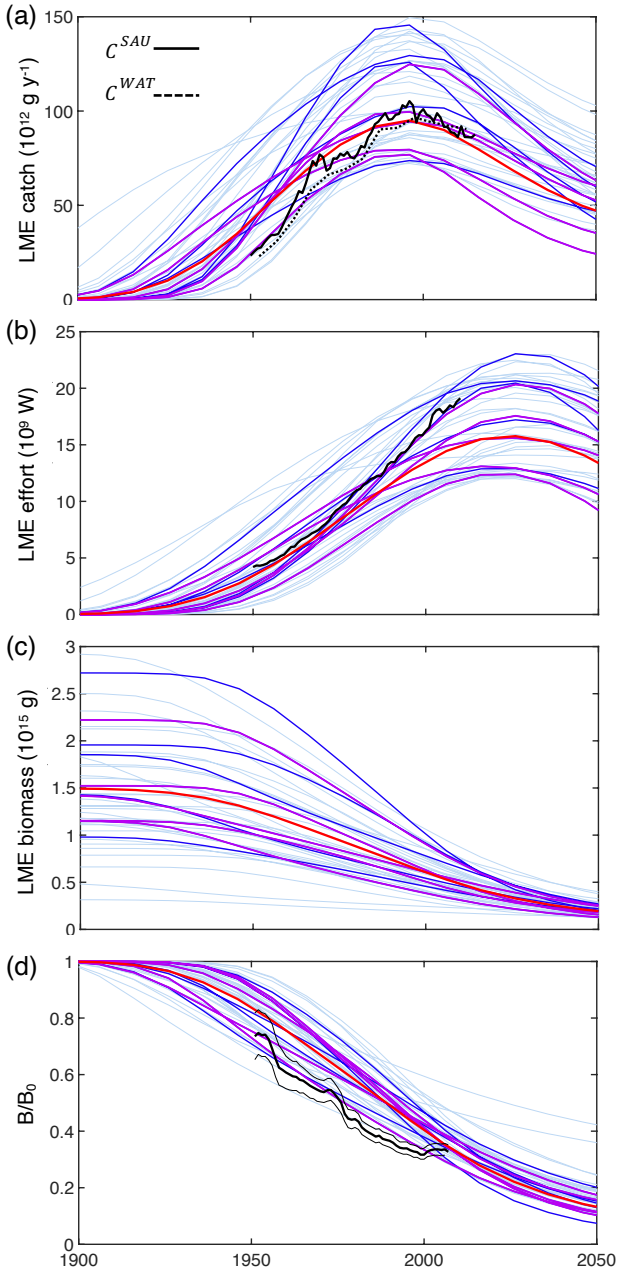

Figure 4. Historical simulations of catch, effort and biomass for the best 42 simulations in the BOATSv2 Monte Carlo ensemble. (a) Catch, (b) nominal effort, (c) biomass, and (d) biomass normalized to initial biomass in the selected 55 LMEs, for the 42 best parameter sets, from 1900 through 2050. Ensembles are aligned at the catch peak of the 1990s. The light blue lines show each parameter set; the dark blue lines show the 10 best simulations out of which the 5 purple lines show the final best ensemble. The thick red line is the mean of the 5 best-ensemble simulations. Black lines in panels (a, b, d) show observational reconstructions, consisting of catch from SAU (black line in panel a, C^{SAU}) and the WAT database (black dotted line in panel a, C^{WAT}), effort (black line in panel b), and biomass from fish stock assessments normalized to the initial state (black line in panel d). Note that the simulations do not include the effects of climate change, environmental variability other than the seasonal cycle, and management.

https://doi.org/10.5194/gmd-2024-26
Preprint. Discussion started: 2 May 2024

Table 3. Sensitivity of model variants for various combinations of ecological and economical processes. We report Pearson coefficients between mean simulated and observed catch across the 55 selected LMEs, at global peak r_{LME90s}, or for historical maximum r_{LMEmax}, and across High Seas Ecosystems (HSEs) at global peak r_{HSE90s}. We report the fraction of high vs. coastal sea catch R_C, and the mean depth of catch $\overline{Z}_C$, in the 1950s and near global peak of the 1990s. The upperscripts SAU and WAT indicate the kind of observation, for pelagic P or demersal D communities with SAU.

Observation or Model version	r^{SAU}_{LME90s}	r^{WAT}_{LME90s}	r^{SAUD}_{LMEmax}	r^{WAT}_{LME90s}	r^{SAU}_{HSE90s}	r^{WAT}_{HSE90s}	$\overline{R}_{C50s}$ $(P;D)$	$\overline{R}_{C90s}$ $(P;D)$	$\overline{Z}_{C50s}$ $(P;D)$	$\overline{Z}_{C90s}$ $(P;D)$
SAU							0.07 (0.10;0.05)	0.09 (0.11;0.07)	188 (266;136)	372 (546;206)
WAT							0.05	0.08	126	154
BOATSv1	0.69	0.73			0.22	0.39	0.11	0.40	445	1698
v1 + α^{corr}	0.50	0.62			0.81	0.71	0.09	0.31	386	1440
v2-Bio* & Π_β)	0.69	0.73	0.46	0.69	0.58	0.67	0.05 (0.13;0.02)	0.16 (0.32;0.07)	179 (273;43)	694 (1001;316)
v2-Bio + $c_k^{corr}(z_{bot})$	0.69	0.73	0.46	0.69	0.59	0.68	0.05 (0.13;0.02)	0.14 (0.31;0.06)	109 (280;36)	571 (991;148)
v2-Bio + $c_k^{corr}(d_{coast})$	0.69	0.73	0.46	0.69	0.51	0.63	0.05 (0.12;0.02)	0.14 (0.28;0.07)	110 (267;43)	555 (873;259)
v2-Bio + $q_k^{corr}(z_{bot}, P)$	0.69	0.74	0.46	0.69	0.56	0.67	0.06 (0.11;0.02)	0.13 (0.27;0.07)	78 (124;37)	526 (827;246)
v2-Bio + $q_k^{corr}(z_{bot}, P$ or $D)$	0.68	0.73	0.46	0.69	0.51	0.64	0.05 (0.11;0.02)	0.10 (0.27;0.05)	47 (79;28)	315 (553;103)
BOATSv2	0.68	0.73	0.46	0.69	0.51	0.64	0.06 (0.10;0.02)	0.11 (0.24;0.06)	75 (121;34)	420 (718;141)

*v2-Bio = v1 + α^{corr} + (Π_ψ

Geoscientific Model Development Discussions
Open Access
EGU

https://doi.org/10.5194/gmd-2024-26
Preprint. Discussion started: 2 May 2024

Geoscientific Model Development Discussions

– (1) At the LME level, heterogeneous costs or catchability have little impact on the regional variability of catch at the time of the global peak ($r^{SAU}_{LME90s} \simeq 0.69$ and $r^{WAT}_{LME90s} \simeq 0.73$, Table 3). The comparison reveals overall better correlations when comparing models with WAT catch reconstructions, where most of the improvement is explained by higher mean catches in Australian LMEs (compare Fig. 5c and d). We also compare the Pearson correlation coefficients of maximum catch by LME for pelagic and demersal catch separately. While heterogeneous costs or catchability show limited impacts, the variability of maximum pelagic yields is less accurately reproduced than maximum demersal yields, $r^{SAUP}_{LMEmax} \simeq 0.46$ vs. $r^{SAUD}_{LMEmax} \simeq 0.69$ (Table 3). This suggests that analogous parameterizations of heterogeneous costs and catchability will generate comparable variability in LME catches.

– (2) Beyond LMEs, in HSEs, Pearson correlation coefficients at peak r_{HSE90s} indicate a significant improvement from BOATSv1 $r_{HSE90s} < 0.39$ (see Table 3) to BOATSv2 $r_{HSE90s} > 0.58$, showing the importance of separating pelagic from demersal pathways to accurately capture the patterns of catch in the open ocean. Introducing specific economic parameterizations results in only minor variations and does not significantly enhance the accuracy of catches in the HSEs.

– (3) There is likely an interplay between heterogeneous catchability and costs. To determine how costs influence the catch fraction in the High Seas, and indirectly the historical offshore expansion of fisheries, we computed the High Sea catch fraction in the 1950s ($\overline{R}_{C50s}$), and near the global catch peak of the 1990s ($\overline{R}_{C90s}$). While we expect $\overline{R}_{C50s} \simeq 0.06$ to increase to only $\overline{R}_{C90s} \simeq 0.09$ at global peak, separate pelagic and demersal energy pathways result in $\overline{R}_{C50s} = 0.05$ and $\overline{R}_{C90s} = 0.16$ (see Table 3). The difference in the 1990s is mostly driven by higher pelagic catch than observed ($\overline{R}_{C90s,P} \simeq 0.32$, compared to 0.11 in observations). Heterogeneous costs, mainly corrected by the distance from shore, improve this fraction ($\overline{R}_{C90s,P} \simeq 0.30$). Note that both cost parameterizations also improve the fraction of demersal catch.

– (4) To better characterize the offshore expansion we also computed the catch-weighted mean depth over which fishing occurs, in the 1950s and 1990s, $\overline{Z}_{C50s-90s}$. For demersal catch ($\overline{Z}_{C50s,D} < 136$ m and $\overline{Z}_{C90s,D} < 206$ m), the mean fishing depth reflects the historical deepening of fishing grounds (Watson and Morato, 2013). For pelagic catch ($\overline{Z}_{C50s,P} < 266$ m and $\overline{Z}_{C90s,P} < 546$ m), it reflects an offshore expansion of fishing effort towards High Seas regions with deeper seafloor. In the model, a rapid offshore expansion of pelagic catch leads to an overestimate of the mean ocean depth at which fishing occurs ($\overline{Z}_{C90s} \simeq 700$, compared to 372 m observed, because $\overline{Z}_{C90s,P} \simeq 1000$ m). Distance-dependent costs slightly improves this discrepancy ($\overline{Z}_{C90s,P} = 873$ m). Depth-dependent costs also contribute to delaying the deepening of demersal catches. Since both depth- and distance-dependent cost parameterizations slightly improve aspects of the simulations, we retain both parameterizations in the final BOATSv2 update.

– (5) Finally, to determine how catchability influences the development of High Seas fisheries, we also compare catch indicators ($\overline{R}_C$ and $\overline{Z}_C$) with observations for heterogeneous parameterizations of catchability. Compared to BOATSv1, increased catchability near seamounts reduces the development of fishing over deep seafloor. This improves $\overline{Z}_{C90s}$,

https://doi.org/10.5194/gmd-2024-26
Preprint. Discussion started: 2 May 2024

Geoscientific Model Development Discussions

especially for pelagic catches ($\overline{Z}_{C90s,P}$ decreases to 553 m, Table 3), and thus significantly reduces their offshore expansion ($\overline{R}_{C90s,P} = 0.27$). However, when this correction is applied both to pelagic and demersal communities, the maximum depth of demersal catch becomes excessively shallow ($\overline{Z}_{C90s,D} = 103$ m). When depth-dependent fishing costs are also included, demersal catches deviate even more from observations. Therefore, we retain the heterogeneous catchability parameterization only for pelagic fishing effort in the final BOATSv2 update.

These findings reveal that the representation of fisheries in coastal seas remains largely comparable between BOATSv1 to BOATSv2, regardless of the details of the economic parameterizations. This confirms that ecological updates primarily contribute to model improvements, while spatially variable costs and catchability only provide minor adjustments. For the final reference simulations with BOATSv2, we included costs that increase with the distance from shore, and costs that increase with seafloor depth for demersal fishing (see Points 3 and 4). We also included catchabilities that decrease with seafloor depth for the pelagic community (see Point 5). This formulation significantly improves the model's ability to reproduce the delayed development of High Seas fisheries, and the progressive deepening of catch (see red lines in Fig. 5a,b).

In summary, at the LME-level, BOATSv2 and BOATSv1 have similar accuracy in their representation of regional catches (see $r_{LME90s} = 0.69/0.73$, Table 3 and Fig. 5c,d). This lack of improvement in the new model version is explained by a limited accuracy in predicting pelagic catches across LMEs (see $r_{LMEmax,P} = 0.46$ vs. $r_{LMEmax,D} = 0.69$, Table 3, and Fig. 5e,f). Nevertheless, BOATSv2 better captures the large scale variability of catches in the HSEs, which are approximately one order of magnitude smaller than in LMEs (see $r_{HSE90s} = 0.51/0.64$, Table 3, and Fig. 5g,h), and better reproduces their historical offshore expansion ($\overline{R}_{C90s} = 0.11$ and $\overline{Z}_{C90s} = 420$ m, Table 3).

5 Results and discussion

5.1 Parameter sensitivity

The best parameter sets selected by the Monte Carlo approach (Section 4.2) provide insights on the functioning of ecological communities. Of the 11 parameters that were optimized for, 6 have a posterior distribution significantly different from the prior distribution (p-values$< 10^{-2}$, Table 1). The posterior distribution for these 6 parameters was also different when optimizing BOATSv1 (see Carozza et al. (2017)), confirming their essential role in influencing the sensitivity of the model.

First, the ensemble mean allometric scaling exponent, $b = 0.72$ (range $[0.70 - 0.80]$ for the 5 best ensemble, see Table 2), is larger than the BOATSv1 value of 0.65 (Carozza et al., 2017), but in the middle of the expected range $0.66 - 0.75$ (Brown et al., 2004; Kooijman, 2010; Hatton et al., 2019). Second, the mortality constant ζ_1 was selected to be slightly negative (-0.07), different from the initial distribution (mean 0.54), and the mortality scaling (0.51) was smaller than the mean value (0.54). To account for a large uncertainty in the trophic efficiency (α) (Eddy et al., 2020), we expanded its prior range to $[0.06, 0.4]$ (compared to previous estimates in Carozza et al. (2017)). However, the optimization persistently selected for values comparable to BOATSv1, with a mean of 0.14 (range $[0.09 - 0.14]$, Table 2). Although separate pelagic and demersal communities could have different trophic efficiencies (Stock et al., 2017; Du Pontavice et al., 2020), here for simplicity we adopt the same value. The

https://doi.org/10.5194/gmd-2024-26
Preprint. Discussion started: 2 May 2024

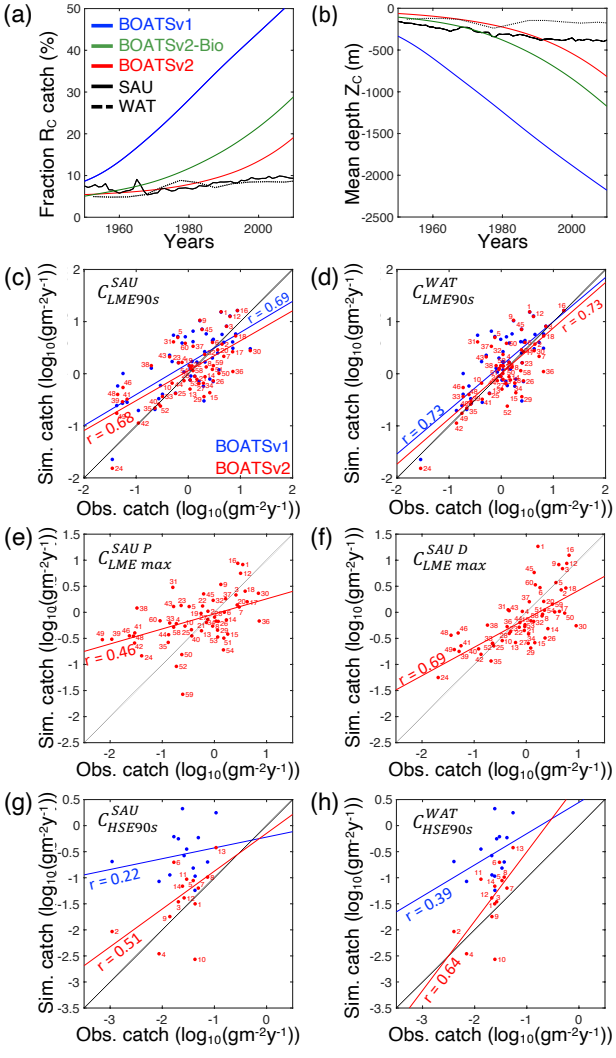

Figure 5. Evaluation of BOATSv2. (a) Observed and simulated historical development of High Seas vs. coastal seas catch R_C. (b) Observed and simulated historical deepening of global catches Z_C. (c,d) Scatter plot of the observed vs. simulated catch at global peak in 55 LMEs, for SAU reconstructions C^{SAU}_{LME90s} in (c), and WAT reconstructions C^{WAT}_{LME90s} in (d). (e,f) Scatter plot of the observed vs. simulated maximum catch in LMEs, for pelagic C^{SAUP}_{LMEmax} in (e), and demersal catch C^{SAUD}_{LMEmax} in (f). (g,h) Scatter plot of the observed vs. simulated catch at global peak in HSEs, for SAU reconstructions C^{SAU}_{HSE90s} in (g), and WAT reconstructions C^{WAT}_{HSE90s} in (h). In panels (a) and (b), SAU and WAT reconstructions are indicated by solid and dotted lines respectively, BOATSv1 by the blue line, BOATSv2-Bio by the green and BOATSv2 in red. In panels (c-h) blue dots and lines show BOATSv1, red dots and lines BOATSv2. Numbers next to each dot indicate the LMEs or HSEs (see regions in Appendix E).

https://doi.org/10.5194/gmd-2024-26
Preprint. Discussion started: 2 May 2024


Geoscientific Model Development Discussions

robustness of the optimized trophic efficiency suggests that sources of variability are captured by other model parameterizations, e.g., the representative size of primary producers, or the temperature dependence of growth and mortality. Lastly, growth activation energies ($\omega_{a,A}$) for pelagic (0.50) and demersal (0.37) communities are larger than the prior values. Although the temperature dependence of mortality ($\omega_{a,\lambda}$) is not significantly different from the initial values, the optimized values suggest a stronger sensitivity of growth compared to mortality for the pelagic community ($\omega_{a,A} - \omega_{a,\lambda} = +0.047$ eV), and a stronger sensitivity of mortality for the demersal community (-0.082 eV).

Covariations between parameters in the 42-member optimized ensemble reveal compensations between parameter pairs (see Fig. 6a). The most significant compensations are between parameters controlling the biomass flow through the size spectrum and biomass losses (see Fig. 6b-d). For instance, an increase in the trophic efficiency (α) can be compensated by a smaller predator-prey biomass ratio (β), which lengthens the food-web (Fig. 6b, $r = -0.66$). When more biomass flows across trophic levels, longer food chains ultimately lead to greater losses over the food-web, and thus similar fish biomass production. Alternatively, an increase in the trophic efficiency can be compensated by an increase of the mortality constant (ζ_1, Fig. 6c, $r = 0.42$). When individual growth limits the biomass flow (Equation 2), a larger growth scaling exponent (b) indirectly allows larger asymptotic sizes (m_∞) that are exposed to larger natural mortality; however, since m_∞ is fixed (Equation 3), ζ_1 decreases to compensate for the increased losses (Fig. 6d, $r = -0.49$).

Correlations between parameters that differ between pelagic and demersal food webs can also reveal trade-offs, particularly in how activation energies collectively affect the two communities (see Fig. 6e-g). For instance, an increased temperature sensitivity of growth for the pelagic community $\omega^P_{a,A}$ is matched by an increased sensitivity of growth for the demersal community $\omega^D_{a,A}$ (Fig. 6e, $r = 0.74$), and a shift of the sensitivity of demersal mortality compared to demersal growth $\omega^D_{a,A-\lambda}$ (Fig. 6f, $r = 0.65$). Another relationship between communities is observed for losses. As the temperature dependence of mortality for the pelagic community ($\omega^P_{a,\lambda}$) increases, increasing losses, there is a concurrent decrease in the representative size at the base of the benthic food chain ($log_{10}(m_\beta)$. This extends the food chain length, increasing losses in the demersal community (Fig. 6g, $r = -0.40$).

While not exhaustive, this parameter analysis suggests trade-offs between biomass production and dissipation in pelagic and demersal communities (see Fig. 6a for further detail).

5.2 Catch

5.2.1 Global catch

Relative to BOATSv1, BOATSv2 corrects for the overestimate of High Seas catches (see Fig. 5) while maintaining a similar skill in reproducing historical variations of LME fish catch (see comparison of model ensemble means with SAU and WAT reconstructions, Fig. 4). BOATSv2 also shows improved skill in hindcasting the spatial evolution of catchs (see Fig. 7), and the offshore and equatorward expansion of fisheries (Swartz et al., 2010; Guiet et al., 2020). In the 1950s (Fig. 7a-c), higher latitude shelf regions and productive upwelling regions contributed the most to global catches. In the 1990s (Fig. 7d-f), while high latitudes still produced large catches, subtropical regions were also significantly exploited, especially in shallow regions.

https://doi.org/10.5194/gmd-2024-26
Preprint. Discussion started: 2 May 2024

Geoscientific Model Development
Discussions
Open Access
EGU

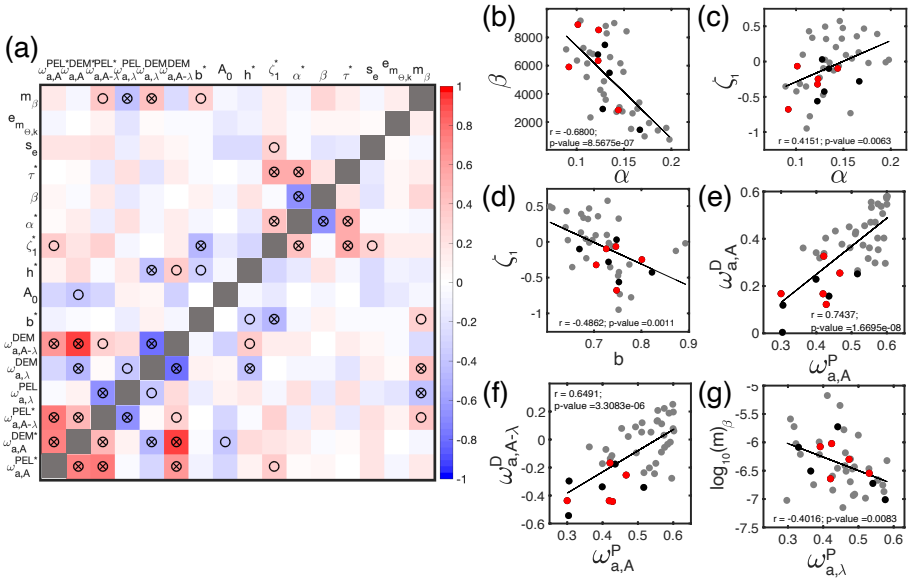

Figure 6. Emergent relationships between model parameters. (a) Pairwise correlations between model parameters for the 42-member optimized ensemble. (b-g) Scatter plots illustrating the relationships between the most strongly correlated parameters: (b) trophic efficiency (α) and predator-prey mass ratio (β); (c) trophic efficiency (α) and mortality constant (ζ_1); (d) growth scaling exponent (b) and mortality constant (ζ_1); (e) growth activation energy for the pelagic community ($\omega^P_{a,A}$) and demersal community ($\omega^D_{a,A}$); (f) growth activation energy for the pelagic community ($\omega^P_{a,A}$) and difference between growth and mortality activation energies ($\omega^D_{a,A-\lambda}$) for the demersal community; (g) mortality activation energy for the pelagic community ($\omega^P_{a,\lambda}$) and representative size of organisms at the base of the demersal food web (m_β). In panel (a), circles indicate p-values<0.05 and stars p-values<0.01. In panels (b-g), the lines show linear regressions for the 42 parameter values of the ensemble; Pearson correlation r and p-values are reported on each plots. In panels (b-g), red dots indicate the 5 final best parameter values for BOATSv2, while the black dots show the remaining 5 parameter values among the 10 best; gray dots indicate all other parameter values.

Productive High Seas areas also supported significant fishing. The expanded representation of ecological processes accounts for most improvements in the High Seas, while updating economic processes only yields minor improvements (see Appendix G).

Despite the closer fit to observations, model biases remain, in particular low offshore catches in the Western Equatorial Pacific, and excessive catches in the Northern and Southern Atlantic (see Fig. 7d). Processes not included in the model, such as habitat alteration by bottom-trawling gears, fish stock migrations, management and regulation likely play a role in these biases. While the observational catch reconstructions used to calibrate the model show differences, likely related to the different methods (e.g., using bathymetry or not, compare Fig. 7e,f), biases in simulated catches remain apparent when comparing with either reconstruction.

Figure 8 shows the differences (residuals) between maximum simulated and observed peak catches in each LME. While there is an overall improvement from BOATSv1 to BOATSv2 (compare Fig. 8a,b to c,d), areas of over- (e.g., Indian Ocean)

https://doi.org/10.5194/gmd-2024-26
Preprint. Discussion started: 2 May 2024

Geoscientific Model Development Discussions

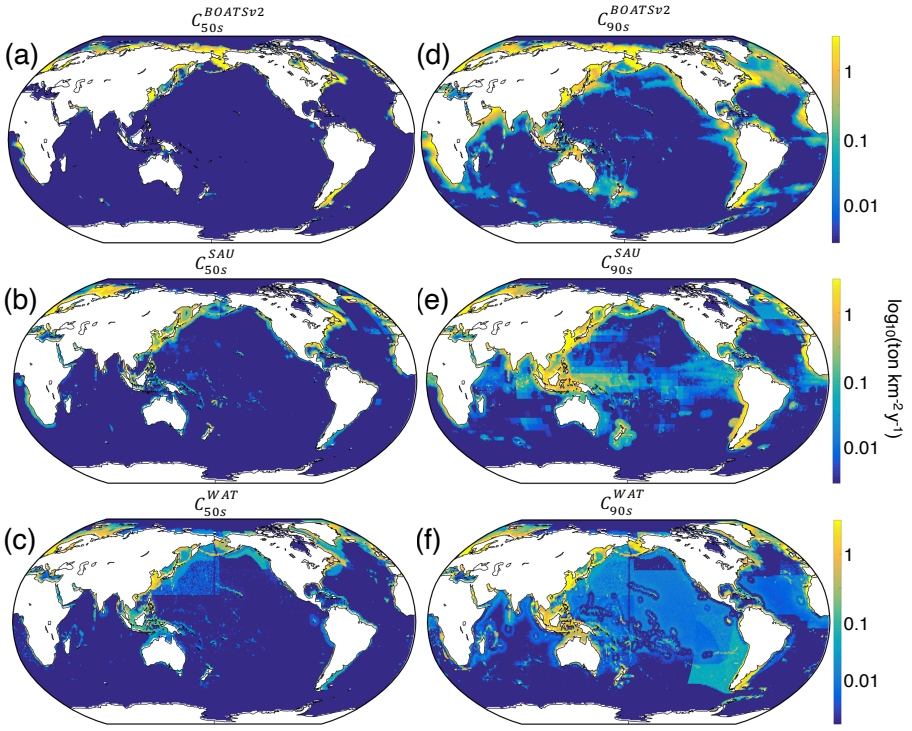

Figure 7. Observed and simulated catch in the 1950s and 1990s $C_{50s-90s}$ (in $\log_{10}(\text{ton km}^{-2}\ \text{y}^{-1})$). (a,d) BOATSv2 simulation compared to (b,e) SAU and (c,f) WAT observation.

or under-estimated catches (e.g., North-West Pacific) are correlated between the two model versions, suggesting remaining structural biases in the model.

5.2.2 Pelagic vs. demersal catch

Separate pelagic and demersal energy pathways allow simulation of higher taxonomic diversity. At the global peak of the 1990s, a large fraction of simulated demersal catch is derived from high latitudes (Fig. 9), in general agreement with observations (van Denderen et al., 2018). At lower latitudes, modeled demersal catches are as abundant as pelagic catches in shallow regions or near seamounts, also consistent with observations. Significant biases remain, however, such as in the North Atlantic, where the simulated demersal catch fraction is lower than observed, and the eastern tropical Pacific, where the demersal fraction is overestimated.

5.2.3 Catch deepening

The historical expansion of fisheries is associated with a deepening of the catch (Morato et al., 2006; Watson and Morato, 2013). This can be attributed to the need to find new profitable fishing grounds beyond more accessible coastal regions, as

https://doi.org/10.5194/gmd-2024-26
Preprint. Discussion started: 2 May 2024

Geoscientific Model Development Discussions

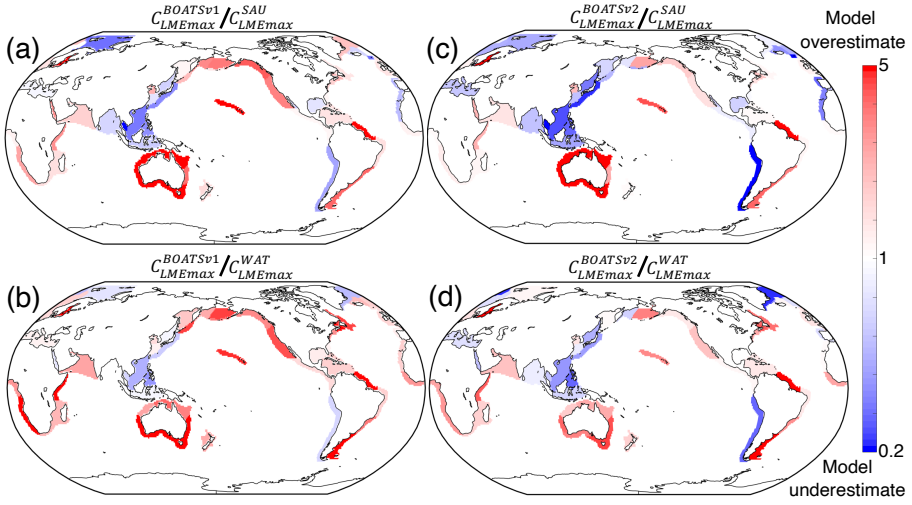

Figure 8. Residuals of observed vs. simulated maximum catch per LME C_{LMEmax} ($log_{10}(C^{sim}/C^{obs})$). (a,b) BOATSv1 simulation compared to SAU and WAT observation. (c,d) BOATSv2 simulation compared to SAU and WAT observation.

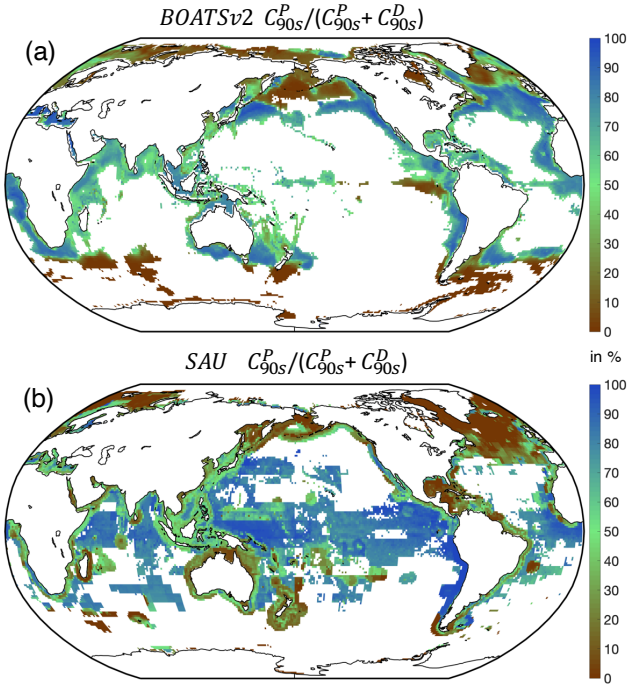

Figure 9. Observed and simulated pelagic catch fraction $C^P_{90s}/(C^P_{90s}+C^D_{90s})$ (in %). (a) BOATSv2 simulated fraction compared to (b) SAU observation. Very low catch levels are masked (i.e., below 10^{-3} g m^{-2} y^{-1}).

https://doi.org/10.5194/gmd-2024-26
Preprint. Discussion started: 2 May 2024

Geoscientific Model Development Discussions

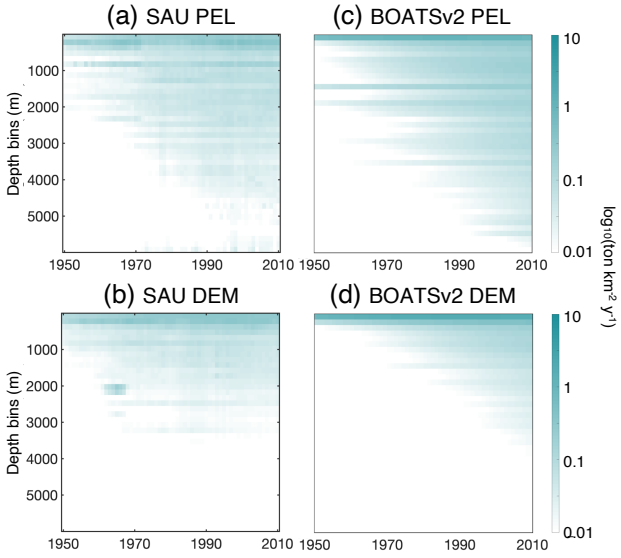

Figure 10. Fishing over increasingly deep seafloors. (a,b) Observed mean catch density (in $\log_{10}(\text{ton km}^{-2}\ \text{y}^{-1})$) over depth stratas for pelagic (a) and demersal (b) catch from SAU. (c,d) Simulated mean catch density over depth stratas for pelagic (c) and demersal (d) catch in BOATSv2 (see Appendix H for comparison with BOATSv1).

well as improvements in fishing technology. The catch density per depth stratum from observational reconstructions reflects such expansion (see Fig. 10a,b for pelagic and demersal catch in SAU data). The deepening of demersal catches is consistent with increasingly deep fishing grounds, while the deepening of pelagic catches indicates an expansion of fishing effort towards deeper regions offshore.

In the model, decreasing biomass with depth slows the historical deepening of demersal catches (Fig. 10d). Similarly, higher costs and reduced catchability at greater depths delay the offshore expansion and deepening of pelagic catches (Fig. 10c). These factors collectively contribute to the slower development of fisheries in deep waters and the reduced catch fraction from the High Seas, consistent with observational reconstructions (compare with BOATSv1 in Appendix H).

5.3 Effort

The modeled nominal effort aggregated across the 55 LMEs broadly matches observations (see observation Fig. 4b), with a slightly earlier decline that falls within the uncertainty range. This could indicate that the model's effort responds to biomass depletion faster than observed, or that the model underestimates the resilience of exploited stocks. It could also reflect the lack of management and subsidies in the model, which influence profitability and the progression of fishing effort.

The significant correlation between modeled and observed effort at peak catch across LMEs (see Fig. 11a, $r_{LME90s} = 0.57$) lends support to the model's assumption of open-access dynamics. However, significant deviations remain (Figure 11b). For instance, the model overestimates effort in highly productive shelf regions near the mouth of major rivers such as the Patag-

https://doi.org/10.5194/gmd-2024-26
Preprint. Discussion started: 2 May 2024

Geoscientific Model Development Discussions
Open Access
EGU

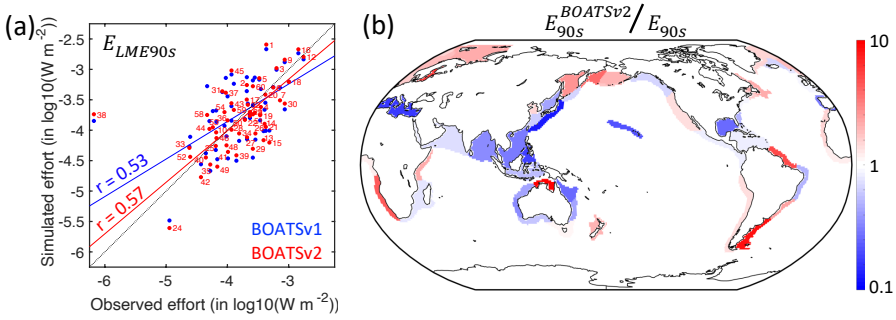

Figure 11. Observed and simulated nominal effort in the 1990s, E_{90s}. (a) Simulated effort density per LME compared to observations E_{LME90s}. (b) Ratio between modeled and observed effort by LME, at the global catch peak in the 1990s. In panel (a), red dots and lines show BOATSv2 output, blue dots and lines BOATSv1 output; numbers indicate the LMEs (see Appendix E).

onian Shelf or North Brazil shelf, suggesting too rapid development of fisheries compared to neighboring regions. Biomass redistribution by currents or fish stock migrations could correct this bias. At larger scales, the model underestimates effort across South-East Asia, consistent with an underestimate of the peak catch. However, effort around Australia is also lower than observed, while the model overestimates catches there (see Fig. 8). This mismatch suggests regional differences in economic drivers, or missing key habitats such as mangroves or reefs. Efficient management might also play a role, although it is unlikely to be the sole driver across the entire region.

5.4 Biomass

5.4.1 Global biomass

In the absence of fishing, BOATSv2 estimates a commercial fish biomass of 1.9 Gton aggregated over LMEs, slightly larger than previous estimates from BOATSv1 (1.6 Gton in Bianchi et al. (2021)). However, because HSE biomass is lower, the LME biomass accounts for 68% of the global biomass (2.8 Gton), significantly more than the 50% of BOATSv1 (3.3 Gton in Bianchi et al. (2021)). Thus, BOATSv2 suggests a $10-15\%$ smaller "pristine" biomass than BOATSv1. When fishing is included and forced by the historically representative catchability increase, the BOATSv2 commercial fish biomass aggregated across LMEs declines by about 50% from 1950 to 2000. This is consistent with both BOATSv1 simulations and global observational estimates (Fig. 4d, also compare with Worm and Branch (2012)). Interestingly, at peak catch, the LME:HSE difference between model versions is compensated by differences in fishing effort, so that both LMEs and HSEs hold approximately 50% of the global biomass at this point (0.9 Gton within LMEs and 0.8 Gton in HSEs with BOATSv2, similar to respectively 0.6 and 0.5 Gton with BOATSv1 (Bianchi et al., 2021)). The optimized parameters of BOATSv2 suggest that the global fish biomass is about 40% pelagic and 60% demersal, a partitioning which could be relevant for the biogeochemical cycling and carbon export effects of fish (Bianchi et al., 2021).

https://doi.org/10.5194/gmd-2024-26
Preprint. Discussion started: 2 May 2024


Geoscientific Model Development Discussions

5.4.2 Regional biomass distributions

In the model, shallow shelves and upwelling systems sustain on average three times more biomass per unit area than the High Seas (10. vs. 2.9 $\mathrm{g\ m^{-2}}$ within and outside the LMEs respectively; see also Fig. 12a for local biomass gradients). Validating these predictions remains challenging because of observational limitations; however recent compilations offer a new means to assess them.

For demersal fish, scientific trawl compilations are now available from the Northern Hemisphere, at locations ranging from Alaska to Europe (Maureaud et al., 2023; van Denderen et al., 2023). Fig. 12 shows that BOATSv2 accurately simulates the average biomass across these LMEs, and captures the biomass increase from the Gulf of Mexico - Florida (GM-FL) to Europe (EU) and North America West coast (NA-W) (see circles Fig. 12b). However, while observations vary over almost two orders of magnitude, simulated biomasses vary only over one order of magnitude. The model also overestimates biomass in the North America East coast (NA-E).

These biases might reflect temporal offsets in the depletion of fish biomass over time due to exploitation (see also Fig. 4d), with the model failing to capture relative differences across LMEs. Indeed, regions where the model overestimates fish biomass still have relatively high simulated rates of biomass decline in the 2000s (e.g., LMEs 1, 5, 12). This can eventually deplete biomass to the observed levels. Conversely, regions where the model underestimates fish biomass (e.g. LMEs 10, 14, 60) are areas in which simulated fishing effort caused an early biomass decline (see Appendix I). These temporal mismatches could reflect regional differences in the rate of development of fisheries that are not captured by the simple, globally homogeneous exponential increase of technology, and by the open access assumption and lack of management. For example, pro-active management in Alaskan fisheries has prevented the phase of overfishing that has been common in many other industrial fisheries worldwide (Worm et al., 2009). Finally, the discrepancies may be exacerbated because observations cover only a portion of each LME (compare mean biomass densities at LME level vs. grid cells where simulations overlap with observations in Appendix I).

Aggregated biomass observations for pelagic stocks are scarcer than for demersal stocks. We compare model output with scientific trawl data for coastal pelagic species in the California Current and Gulf of Alaska (shown by squares in Fig. 12b) (Zwolinski et al., 2012). The model simulates overall higher biomass densities than observed, showing a wider ranges of values. Similar to observations, simulated pelagic biomass densities are lower compared to demersal biomass. A caveat to this comparison is that estimates of pelagic biomass remain significantly uncertain due to challenges in sampling the three-dimensional oceanic environment, variability and aggregation in fish populations, uncertainty in sampled depth ranges, net avoidance by pelagic fish, and the limited selectivity of pelagic trawls (Kaartvedt et al., 2012; Zwolinski et al., 2012). In addition, fish migrations can redistribute fish biomass across life stages in ways not captured by the model.

5.5 Implications of the model update

The inclusion of distinct energy pathways and spatially variable economic drivers in BOATSv2 has a limited impact on the evolution of coastal fisheries over time, but has a large impact on simulated High Seas fisheries. All else being equal, BOATSv1

https://doi.org/10.5194/gmd-2024-26
Preprint. Discussion started: 2 May 2024

Geoscientific Model Development Discussions
Open Access
EGU

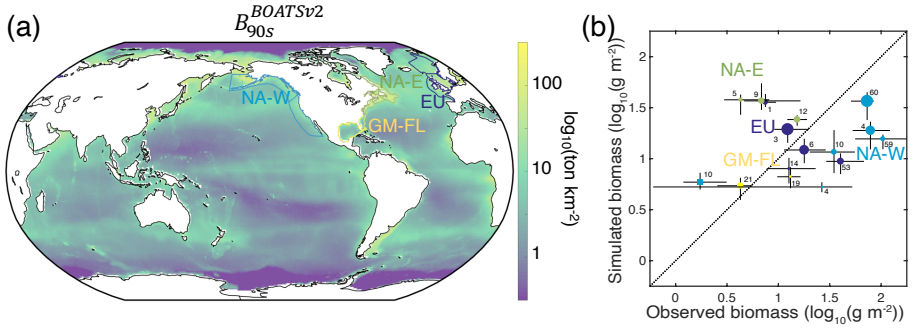

Figure 12. Observed and simulated biomass density. (a) BOATSv2 global mean biomass density in the 1990s, B_{90s}. (b) Demersal biomass density from bottom trawl surveys (circles) versus simulations, and pelagic biomass density from surface coastal pelagic species trawl data (squares) versus simulations. Biomass densities are averaged across LMEs for the reference decade of the 2000s. In panel (b), colors indicate the four different regions shown by the LME boundaries in panel (a), and numbers the specific LMEs (see Appendix E). In panel (b) the dots indicate median values, and horizontal or vertical lines the 25-75th percentile range; the size of the dots indicates the relative size of the surface area sampled. Appendix I provides a further comparison of biomass time-series by LME.

and BOATSv2 ensembles show very similar LME-level catch at global peak (see $C_{LME90s}^{SAU-WAT}$ Fig. 5c,d) and comparable progression across LMEs from 1950 through 2000. Both are in good agreement with observations (Fig. 13). The key improvement of BOATSv2 is the representation of High Seas fisheries, where catches are delayed and greatly reduced during the historical period, bringing the model closer to observations (see dashed lines Fig. 13).

The separation between pelagic and demersal communities influences fish production rates, because these communities respond to different environmental drivers (van Denderen et al., 2021; Fredston et al., 2023). Compared to BOATSv1, this change could influence the resilience of fisheries to fishing and/or climate change. It could also alter the response to regulation, although we anticipate similar dynamics as in previous work (Scherrer and Galbraith, 2020; Scherrer et al., 2020). A separation of pelagic and demersal energy pathways is likely to impact the effects of fish on biogeochemistry (Bianchi et al., 2021; Le Mézo et al., 2022).

6 Conclusions

We introduce BOATSv2, an expanded version of the BOATS model that separates demersal from pelagic communities and improves simulation of High Sea fisheries. New model features have little impact in coastal regions, so that BOATSv2 simulates dynamics and variability in catch and biomass over LMEs that are similar to BOATSv1. The expanded representation of functional and taxonomic diversity allows more detailed comparisons with observations. In some cases, this reveals new model biases, such as in the simulation of demersal catches and biomass in the Western North Atlantic.

We attribute improvements in the simulation of High Seas fisheries to the separation of pelagic and demersal energy pathways, supporting the importance of distinguishing these communities (Blanchard et al., 2012; Petrik et al., 2019; Du Pontavice

https://doi.org/10.5194/gmd-2024-26
Preprint. Discussion started: 2 May 2024

Geoscientific Model Development Discussions
Open Access
EGU

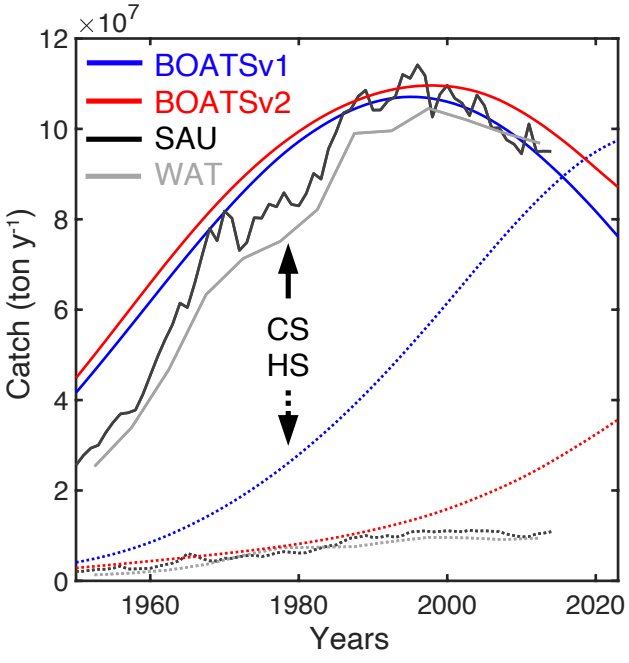

Figure 13. Time-series of catch in the global ocean. Historical annual catch in the High Seas (HS) vs. coastal seas (CS). Gray lines show observational reconstructions from Pauly et al. (2020) (SAU, dark gray), and Watson (2017) (WAT, light gray). Blue lines show output from BOATSv1, and red lines from BOATSv2. Coastal (solid lines) and High Seas (dotted lines) catches are shown separately.

et al., 2020). We also introduced parameterizations of spatially heterogeneous economic drivers, i.e., fishing costs and catchability, which further improves the match with observations in the High Seas. However, choosing between different formulations for these drivers (i.e., depending on distance from the coast, d_{coast}, or depth of the seafloor, z_{bot}) was only possible by testing plausible functional forms and retaining those leading to the largest improvements against empirical data. While this selection was not exhaustive, our final formulation is consistent with recent observations, such as the effect of seamount on fishing effort distributions (Kerry et al., 2022), and the historical deepening of fishing as technology progresses (Watson and Morato, 2013). We acknowledge that the specific choice of functional forms for these parameterizations is not well constrained, and will likely require future refinement against observational diagnostics.

Because of the more accurate representation of High Sea fisheries in BOATSv2 relative to BOATSv1, the fraction of catch that takes place in the High Seas at the time of the global catch peak is reduced from 31% to 11%, bringing it closer to the observed $8-9\%$. Similarly, the mean depth of the catch shoals from 1698 m in BOATSv1 to 420 in BOATSv2, aligning it to the empirical estimate of $154-372$ m. This update should help reduce model uncertainties in future projections (Galbraith et al., 2017; Lotze et al., 2019; Tittensor et al., 2021), and provide a more accurate representation of the role of fish in global biogeochemical cycles (Bianchi et al., 2021; Le Mézo et al., 2022). Future model improvements could include a representation of the movement of fish stocks (Sumaila et al., 2015), the role of diverse coastal environments such as mangroves, reefs, and

https://doi.org/10.5194/gmd-2024-26
Preprint. Discussion started: 2 May 2024

lagoons (Tittensor et al., 2010), and a representation of distinct mesopelagic communities (Irigoien et al., 2014; St. John et al., 2016; Hidalgo and Browman, 2019).

Code availability. The code of the model, forcing to complete reference simulations, and observation to compare the model are available through Zenodo (DOI:https://doi.org/10.5281/zenodo.11043334).

https://doi.org/10.5194/gmd-2024-26
Preprint. Discussion started: 2 May 2024


Geoscientific Model Development Discussions
Open Access
EGU

Appendix A: BOATSv2 governing equations and parameters

https://doi.org/10.5194/gmd-2024-26
Preprint. Discussion started: 2 May 2024

Geoscientific Model Development Discussions

Table A1. List of ecological and economic parameters in BOATSv2, for pelagic (P), demersal (D), or both communities. Parameters selected by the Monte Carlo procedure are reported by the range of best selected values. See more details in Carozza et al. (2016, 2017).

Parameter	Name	Value [Range]	Unit
m_0	Lower bound of smallest mass class	10	g
m_u	Upper bound of largest mass class	100000	g
n_k	Number of fish size groups	3	Unitless
$m_{\infty,k}$	Asymptotic mass of group k	(0.3, 8.5, 100)	kg
T_r	Reference temperature of $a(T)$	10	°C
k_B	Boltzmann's constant	8.617×10^{-5}	eV K^{-1}
$\omega_{a,A}$	Growth activation energy of metabolism	P: [0.30,0.47]; D: [0.12,0.33]]	eV
$\omega_{a,\lambda}$	Mortality activation energy of metabolism	P: [0.39,0.53]; D: [0.49,0.61]]	eV
b	Allometric scaling exponent	[0.70,0.80]	Unitless
A_0	Allometric growth constant	[4.35,5.04]	g^{1-b} s^{-1}
ϵ_a	Activity fraction	0.8	Unitless
c_s	Slope parameter of s_k	5	Unitless
η	Ratio of mature to asymptotic mass	0.25	Unitless
α	Trophic efficiency	[0.09,0.14]	Unitless
β	Predator to prey mass ratio	[2830,8890]	Unitless
τ	Trophic scaling	[-0.27,-0.23]	Unitless
m_L	Mass of large phytoplankton	4×10^{-6}	g
m_S	Mass of small phytoplankton	4×10^{-15}	g
k_E	Eppley constant for phytoplankton growth[1]	0.06	° C^{-1}
Π^*	Nutrient concentration[1]	0.35	mmol C m^{-3} d^{-1}
m_β	Representative mass of benthos	$[8.3 \times 10^{-7}, 1.6 \times 10^{-6}]$	g
b_a	Martin curve attenuation coefficient	-0.8	Unitless
z_{eu}	Reference euphotic layer depth	75	m
$k_{NO_3^-}$	Nitrate concentration constant	5	µM
ζ_1	Mortality constant	[-0.68,-0.07]	Unitless
h	Allometric mortality scaling	[0.46,0.55]	Unitless
Φ_f	Fraction of females	0.5	Unitless
$\Phi_{C,k}$	Fraction of NPP allocated to a group k	1/3	Unitless
s_e	Eggs to recruit survival fraction	[0.024,0.093]	Unitless
m_e	Egg mass	5.2×10^{-4}	g
κ_e	Fleet dynamics parameter	10^{-6}	W $\$^{-1}$ s^{-1}
κ_s	Regulation response parameter	4×10^8	m^2 s^{-1}
S	Societal enforcement strength (here deactivated)	0	Unitless
c_σ	Fishing selectivity slope	17.8	Unitless
$d_{m_{\Theta,k}}$	Selectivity mass adjustment	(1, 1, 1)	Unitless
$e_{m_{\Theta,k}}$	Selectivity mass scaling	[0.44,0.97]	Unitless
(δ_z, δ_d)	Rate of cost increase with depth - distance	$(2.5 \times 10^{-3}, 7.9 \times 10^{-3})$	($\$$ m^{-1} W^{-1} y^{-1}, $\$$ km^{-1} W^{-1} y^{-1})
(z_{ref}, d_{ref})	Reference variables for cost profiles	(200,370)	(m,km)
q_{min}	Minimum gear efficiency	0.8	Unitless
(z_{mean}, z_{max})	Reference depths for catchability profile	(2372,5750)	m

[1] For estimation of the fraction of large phytoplankton production following Dunne et al. (2005).

https://doi.org/10.5194/gmd-2024-26
Preprint. Discussion started: 2 May 2024

Geoscientific Model Development Discussions

Table A2. Variables and governing equations for the ecological module of BOATSv2, for pelagic (P), demersal (D), or both communities. See more details in Carozza et al. (2016, 2017).

Variable and functions	Formulation	Unit
Size (mass) of fish	m	g
Time	t	s
Temperature	$T(t)\begin{cases}\text{P}: T_{75}\\ \text{D}: T_{bot}\end{cases}$	K or °C
Surface nitrate concentration	$NO_3(t)$	µM
Net primary production	$\Pi_\psi(t)$	mmol C m^{-2} s^{-1}
Bathymetry	z_{bot}	m
Fraction of large phytoplankton production[1]	$\Phi_L(t)$	-
Particle export ratio[1]	$pe_{ratio}(t)$	-
Fish biomass spectrum of group k	$f_k(m,t)$	g m^{-2} g^{-1}
Cumulative biomass of group k	$B_k(t)=\int_{m_0}^{m_{\infty,k}} f_k dm$	g m^{-2}
Fish catch spectrum of group k	$h_k(m,t)$	g m^{-2} g^{-1} s^{-1}
McKendrick von Foerster model	$\frac{\partial f_k}{\partial t}=-\frac{\partial \gamma_{S,k} f_k}{\partial m}+\frac{\gamma_{S,k} f_k}{m}-\Lambda_k f_k - h_k$	-
Recruitment at $m=m_0$	$\gamma_{S,k} f_k = R_{P,k}\frac{R_{e,k}}{R_{P,k}+R_{e,k}}$	g m^{-2} s^{-1}
Individual growth rate	$\gamma_{S,k}=(1-\Phi_k)\xi_{I,k}$	g s^{-1}
Fraction of input energy allocated to growth	$\Phi_k = s_k\frac{1-\epsilon_a}{(m/m_{\infty,k})^{(b-1)}-\epsilon_a}$	-
Individual level total energy input	$\xi_{I,k}=\min\left[\frac{\phi_{C,k}\pi m}{f_k}, Am^b - k_a m\right]$	g s^{-1}
Growth constant	$A=A_0 a_A(T)$	g^{1-b} s^{-1}
Mass specific investment in activity	$k_a = A\epsilon_a m_{\infty,k}^{b-1}$	s^{-1}
Fish production spectrum	$\pi=\begin{cases}\text{P}: \frac{\Pi_\psi}{m_\psi}\left(\frac{m}{m_\psi}\right)^{\tau-1}\\ \text{D}: \frac{\Pi_\beta}{m_\beta}\left(\frac{m}{m_\beta}\right)^{\tau-1}\end{cases}$	g m^{-2} g^{-1} s^{-1}
Representative mass of phytoplankton	$m_\psi = m_L^{\Phi_L} m_S^{1-\Phi_L}$	g
Particle flux at bottom	$\Pi_\beta = \Pi_\psi\, pe_{ratio}\left(\frac{z_{bot}}{z_{eu}}\right)^{b_a}$	mmol C m^{-2} s^{-1}
Mass structure of energy to reproduction	$s_k=\left[1+\left(\frac{m}{m_{\alpha,k}}\right)^{-c_s}\right]^{-1}$	-
Mass of maturity	$m_{\alpha,k}=\eta\, m_{\infty,k}$	g
Natural mortality rate	$\Lambda_k = \lambda m^{-h} m_{\infty,k}^{h+b-1}$	s^{-1}
Mortality constant	$\lambda = e^{\zeta_1}\left(\frac{A_0}{3}\right)a_\lambda(T)$	g^{1-b} s^{-1}
Primary production determined recruitment	$R_{P,k}=\Phi_{C,k}\pi(m_0)m_0$	g m^{-2} s^{-1}
Eggs production determined recruitment	$R_{e,k}=\Phi_f s_e \frac{m_0}{m_e}\int_{m_0}^{m_{\infty,k}}\gamma_{R,k}(m)\frac{f_k(m)}{m}dm$	g m^{-2} s^{-1}
Energy allocated to reproduction	$\gamma_{R,k}=\Phi_k\xi_{I,k}$	g s^{-1}
van't Hoff-Arrhenius equation	$a_{a,\lambda}(T)=exp\left[\frac{\omega_{a,\lambda}}{k_B}\left(\frac{1}{T_r}-\frac{1}{T}\right)\right]$	-
Corrected trophic scaling[2]	$\tau=\frac{log\left(\alpha\frac{k_{NO_3^-}}{k_{NO_3^-}+NO_3^-}\right)}{log(\beta)}$	-

[1] Estimated from net primary production and surface temperature following Dunne et al. (2005).

[2] Correction of trophic scaling when reduced growth in iron limited regions is activated.

https://doi.org/10.5194/gmd-2024-26
Preprint. Discussion started: 2 May 2024

Geoscientific Model Development Discussions
Open Access
EGU

Table A3. Variables and governing equations for the economic module of BOATSv2, for pelagic (P), demersal (D), or both communities. See more details in Carozza et al. (2016, 2017).

Variable and functions	Formulation	Unit
Fish catchability of group k	$q_k(t)$	$\mathrm{m^2\ Ws^{-1}}$
Ex-vessel fish price for group k	$p_k(t)$	$\mathrm{\$\ g^{-1}}$
Cost per unit effort for group k	$c_k(t)$	$\mathrm{\$\ W^{-1}\ s^{-1}}$
Bathymetry	z_{bot}	m
Distance to shore	d_{coast}	km
Societal target for fishing effort[1]	$E_{targ,k}(t)$	$\mathrm{W\ m^{-2}}$
Fish catch spectrum of group k	$h_k(m,t)$	$\mathrm{g\ m^{-2}\ g^{-1}\ s^{-1}}$
Cumulative catch of group k	$C_k(t) = \int_{m_0}^{m_{\infty,k}} h_k dm$	$\mathrm{g\ m^{-2}\ s^{-1}}$
Fishing effort of group k	$E_k(t)$	$\mathrm{W\ m^{-2}}$
Fishing effort model	$\frac{dE_k}{dt} = \left(\kappa_e \frac{revenue_k - cost_k}{E_k}\right) e^{-S} + (1-e^{-S})\kappa_s(E_{target,k} - E_k)$	-
Revenue from fishing	$revenue_k = q_k\ E_k\ dt\ \int_{m_0}^{m_{\infty,k}} p_k \sigma_k(m) f_k(m) dm$	$\mathrm{\$\ m^{-2}\ s^{-1}}$
Size dependent selectivity of catch	$\sigma_k = \left[1 + \left(\frac{m}{m_{\Theta,k}}\right)^{-c_\sigma/3}\right]^{-1}$	-
Threshold mass for catch	$m_{\Theta,k} = d_{m\Theta,k}\ e_{m\Theta,k}\ m_{\alpha,k}$	g
Cost of fishing	$cost_k = c_k\ E_k\ dt$	$\mathrm{\$\ m^{-2}\ s^{-1}}$
Corrected depth dependent cost profile[2]	$c_k(z_{bot}) = c_k + \delta_z(z_{bot} - z_{ref})$	$\mathrm{\$\ W^{-1}\ s^{-1}}$
Corrected distance dependent cost profile[2]	$c_k(z_{dist}) = c_k + \delta_d(d_{coast} - d_{ref})$	$\mathrm{\$\ W^{-1}\ s^{-1}}$
Corrected depth dependent catchability profile[2]	$q_k(z_{bot}) = q_k\ Pr(z_{bot})\ Of(P,D)$	$\mathrm{m^2\ Ws^{-1}}$
Depth dependent catchability weight	$Pr(z_{bot}) = q_{min} + (1-q_{min})\frac{log_{10}(z_{max}) - log_{10}(z_{bot})}{log_{10}(z_{max}) - log_{10}(z_{mean})}$	-
Catchability offset between communities	$Of(P) = 1.4\ Of(D)$	-

[1] Not detailed in the present model description, see Scherrer and Galbraith (2020).

[2] Correction of catchability or cost when spatial economic parameterization is activated.

https://doi.org/10.5194/gmd-2024-26
Preprint. Discussion started: 2 May 2024

Geoscientific Model Development Discussions
Open Access
EGU

Appendix B: Global variability in surface nitrate

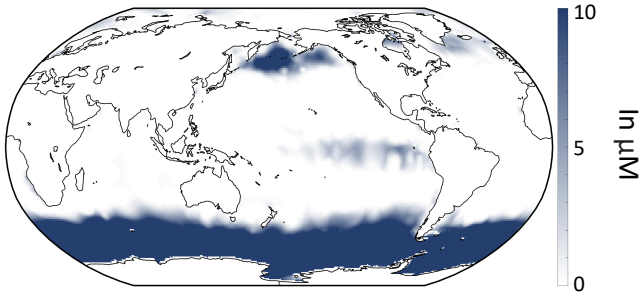

Figure B1. Minimum monthly sea surface nitrate concentration (in µM) from the World Ocean Atlas (Locarnini et al., 2006).

https://doi.org/10.5194/gmd-2024-26
Preprint. Discussion started: 2 May 2024

Geoscientific Model Development Discussions
Open Access
EGU

Appendix C: Spatial variation of costs

The cost of fishing varies by fishing gear and by targeted fish community (Lam et al., 2011). To best constrain spatially variable costs we use estimates of these separate fishing costs in the High Seas for the main gear types (98% of total effort) following data reported by Sala et al. (2018). Table C1 summarizes these estimated costs. These compare with BOATS's default fishing cost of 5.85 \$ W^{-1} y^{-1} (Carozza et al., 2017; Galbraith et al., 2017). We defined spatially variable costs as a function of distance to coast d_{coast}, and depth of the seafloor z_{bot}. Figure C1a illustrates the profile of distance dependent costs and figure C1b the profile of depth dependent costs (in \$ W^{-1} y^{-1}).

Table C1. Cost of fishing the high-seas based on estimates from Sala et al. (2018) for year 2016.

Gear type	Effort in kWh (fraction of total)	Cost range in \$	Cost per unit effort in \$ W^{-1} y^{-1}
Trawlers	979 10^6 (15%)	[750 10^6-1030 10^6]	[6.7-9.2]
Long liners	3719 10^6 (55%)	[2523 10^6-3023 10^6]	[6.0-7.1]
Purse seiners	394 $10^6 s$ (6%)	[702 10^6-1188 10^6]	[15.7-26.0]
Squid jiggers	1490 10^6 (22%)	[1308 10^6-1616 10^6]	[7.7-9.5]
Range all gears	(98%)	-	[6.94-8.87]
BOATS default	-	-	5.85

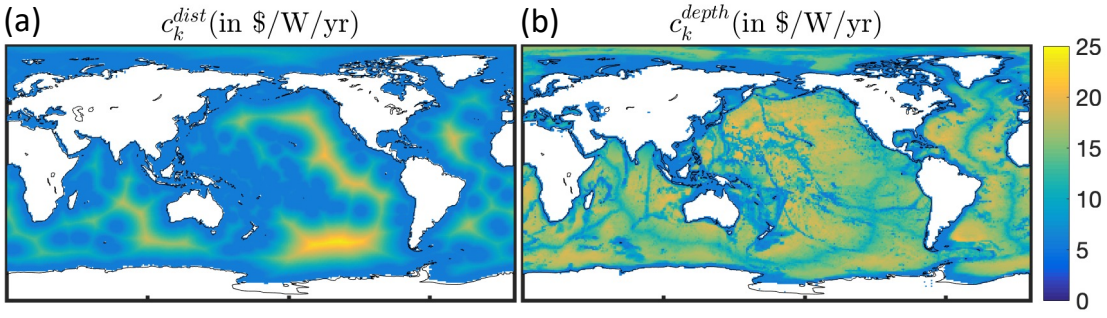

Figure C1. Cost per unit effort profiles c_k^{coor} in the global ocean (in \$ W^{-1} y^{-1}). (a) As a function of distance to the nearest coast $c_k^{coor} = c_k^{dist}$. (b) As a function of depth of the seafloor $c_k^{coor} = c_k^{depth}$.

https://doi.org/10.5194/gmd-2024-26
Preprint. Discussion started: 2 May 2024

Geoscientific Model Development Discussions

Appendix D: Spatial variation of catchability

Technology coefficients varies between gears (Palomares and Pauly, 2019), and gears are predominantly used in separate regions of the global ocean (Kroodsma et al., 2018; Kerry et al., 2022). Ultimately this can lead to spatially heterogeneous catchability of fish resource.

In order to better constrain the catchability, we use the reported difference of technology coefficients by gear estimated in 1995, and a coarse estimation of the contribution of each gear to the global fishing effort from 2015 through 2020 as reconstructed by Global Fishing Watch (GFW, see Kroodsma et al. (2018)). Depending on the functional type predominantly targeted by a gear, pelagic vs. demersal, we estimate the mean technology coefficients for pelagic species to be $Of(P) = 1.3$ compared to $Of(D) = 0.9$ for demersal species (see Table D1).

Based on the observation that a dominant part of fishing effort on pelagic species by longliners occurs near seamounts (Kerry et al., 2022), we adjust the spatial catchability as a function of the depth of the seafloor such that it varies from a minimum of $Pr(z_{bot}) = 0.8$ over deep seafloors (e.g., for tuna seiners, Table D1) to $Pr(z_{bot}) = 2.4$ in shallow regions (such that the global mean is 1.3). Figure D1 illustrates the reference profile of technology coefficients $Pr(z_{bot})$ used for the analysis.

Table D1. Technology coefficient per fish community. The coefficients per gear are based on reported values in Palomares and Pauly (2019). Each gear is linked to the dominant resource it targets, pelagic (Pel) or demersal (Dem), and associated to the fraction of global fishing effort from 2015 through 2020, as reported by Global Fishing Watch. We reported the mean technological coefficient weighted with effort by gear, when available.

Gear type (fraction of GFW effort)	Dominant target (Pel vs. Dem)	Technology coefficient 1995 (normalized)
Super trawlers (-)	Pel	1.3
Tuna seiner (1.1%)	Pel	0.8
Freeze trawler (-)	Pel	1.0
Tuna longliner (-)	Pel	1.2
Purse seiner (2.2%)	Pel	1.0
Stern trawler (-)	Pel/Dem	1.0
Longliner (19%)	Pel	1.4
Multipurpose vessel (-)	Pel/Dem	1.3
Shrimp trawler (-)	Dem	1.1
Trawler (48%)	Dem	0.9
Gillnetter (6%)	Dem	0.8
Fast potter (0.7%)	Dem	0.7
Other (23%)	Pel/Dem	–
Mean pelagic (22%)	Pel	1.3
Mean demersal (55%)	Dem	0.9

https://doi.org/10.5194/gmd-2024-26
Preprint. Discussion started: 2 May 2024

Geoscientific Model Development Discussions
Open Access
EGU

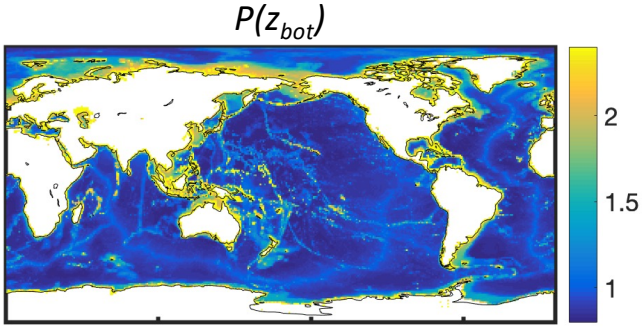

Figure D1. Relative technology coefficient profiles $Pr(z_{bot})$ in the global ocean.

https://doi.org/10.5194/gmd-2024-26
Preprint. Discussion started: 2 May 2024

Geoscientific Model Development Discussions
Open Access
EGU

Appendix E: Large Marine Ecosystems and High Seas Ecosystems

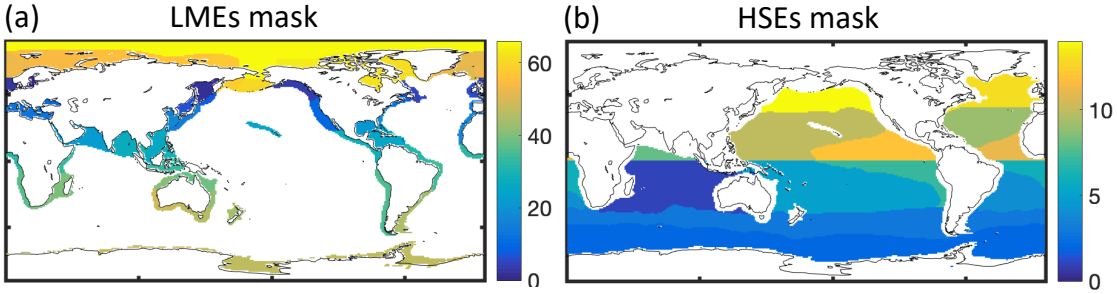

Figure E1. Regional masks used to compare observations and simulations. (a) Large Marine Ecosystems. (b) High Seas Ecosystems adapted from Weber et al. (2016).

https://doi.org/10.5194/gmd-2024-26
Preprint. Discussion started: 2 May 2024

Geoscientific Model Development Discussions
Open Access
EGU

Appendix F: Pelagic and Demersal catches

Table F1. Association of Sea Around Us (Pauly et al., 2020) functional types to pelagic and demersal catches.

Catch type	SAU functional types
Pelagic	pelagic s/m/l
	bathypelagic s/m/l
	cephalopods
Demersal	demersal s/m/l
	reef-associated s/m/l
	benthopelagic s/m/l
	bathydemersal s/l
	shark s/l
	flatfish s/l
	ray s/l
	shrimp
	lobster and crab
	other demersal invertebrates

https://doi.org/10.5194/gmd-2024-26
Preprint. Discussion started: 2 May 2024

Geoscientific Model Development Discussions
Open Access
EGU

Appendix G: Global catch distribution between BOATS versions

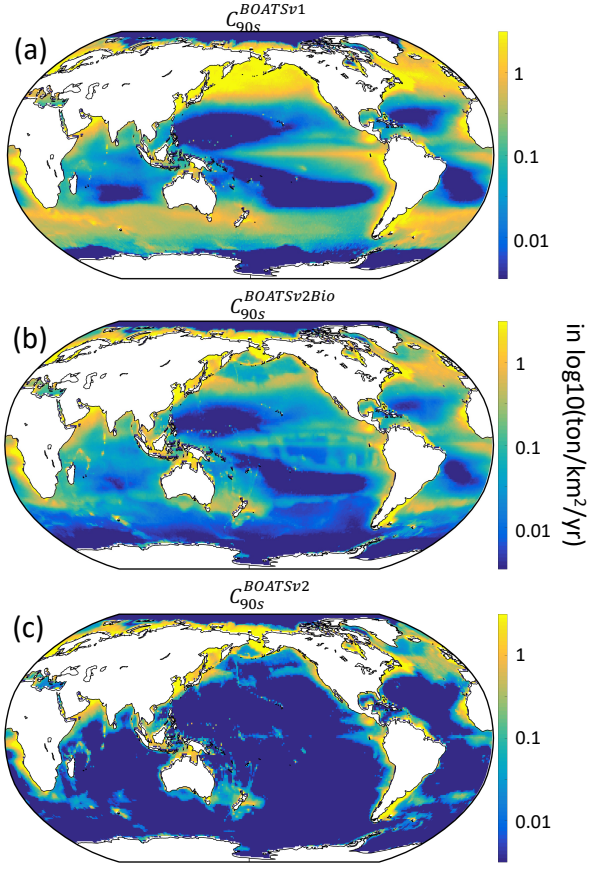

Figure G1. Simulated catch in the 1990s C_{90s} (in $\log_{10}(\text{ton km}^{-2}\,\text{y}^{-1})$). (a) BOATSv1. (b) Updated version with improved ecology BOATSv2-Bio. (c) Final update including improved economics BOATSv2.

https://doi.org/10.5194/gmd-2024-26
Preprint. Discussion started: 2 May 2024

Geoscientific Model Development Discussions
Open Access
EGU

Appendix H: Historical catch deepening

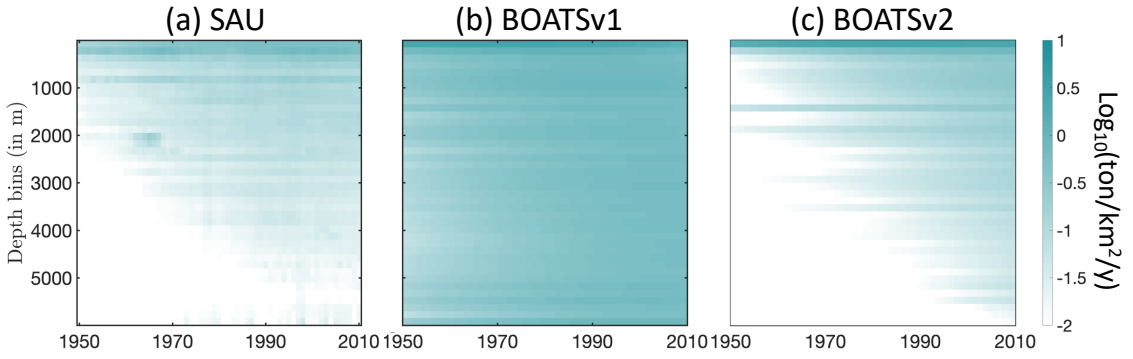

Figure H1. Fishing over increasingly deep seafloors. (a) Observed and (b,c) simulated mean total catch density (in $\log_{10}(\text{ton km}^{-2}\,\text{y}^{-1})$) over depth strata. Compared to observation (a), BOATSv1 (b) fail to capture the deepening while BOATSv2 corrects it.

https://doi.org/10.5194/gmd-2024-26
Preprint. Discussion started: 2 May 2024

Geoscientific Model Development Discussions

Appendix I: Historical biomass variation in selected LMEs

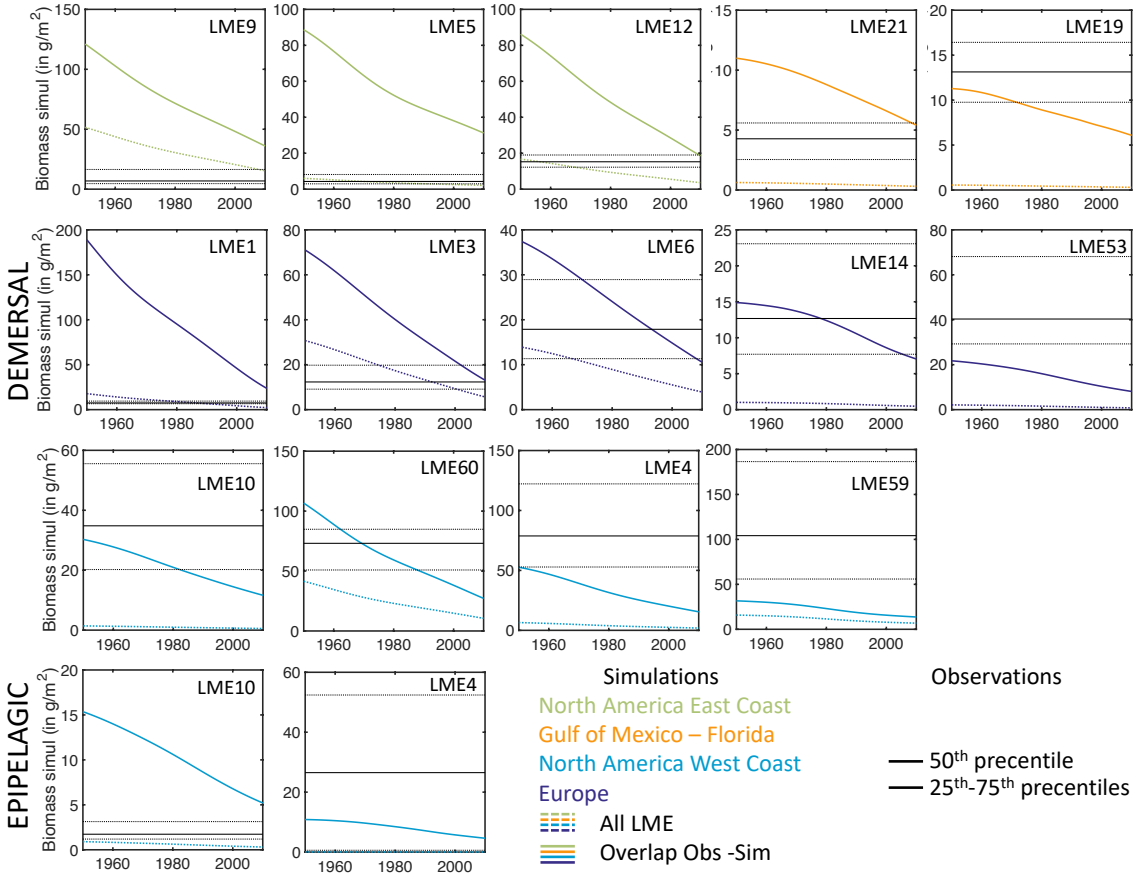

Figure I1. Observed and simulated biomass decline in LMEs, for demersal and pelagic biomass. Each panel shows the simulated historical fish biomass density (in g m^{-2}) decline, averaged across the selected LME (dotted line), or averaged over 1^o grid cells where observation are available (plain line). These are compared to the range of observed biomass density per LME over years 2000s, indicated by the median value (black plain lines) and the $25th$ and 75th percentiles (dotted black lines). Colors indicate neighboring LMEs, North American LMEs along the East coast (green), North American LMEs along the West coast (light blue), Gulf of Mexico and Florida LMEs (in orange), European LMEs (dark blue).

Author contributions. J.G., D.B., K.J.N.S., R.F.H. and E.D.G. discussed and designed the new model developments and analysis. J.G. implemented the code updates and merged past developments from K.J.N.S., D.B., and E.D.G.. J.G. performed the simulations and analysis. J.G. wrote the first draft and prepared the figures and tables in collaboration with D.B.. All authors provided critical feedback on the results and contributed to the final manuscript.

https://doi.org/10.5194/gmd-2024-26
Preprint. Discussion started: 2 May 2024


Geoscientific Model Development Discussions

Competing interests. The authors declare that they have no conflict of interest.

Acknowledgements. D.B. and J.G. acknowledge support from the US National Aeronautics and Space Administration (NASA) grant 80NSSC21K0420. Computational resources were provided by the Expanse system at the San Diego Supercomputer Center through allocation TG-OCE170017 from the Advanced Cyber infrastructure Coordination Ecosystem: Services and Support (ACCESS) program, which is supported by National Science Foundation grants 2138259, 2138286, 2138307, 2137603, and 2138296. E.D.G. was supported by the Canada Research Chairs Program fund number CRC-2020-00108. K.J.N.S. was supported by the Norwegian Research Council, project 326896.

https://doi.org/10.5194/gmd-2024-26
Preprint. Discussion started: 2 May 2024

Geoscientific Model Development Discussions
Open Access
EGU

References

Amante, C. and Eakins, B. W.: ETOPO1 arc-minute global relief model: procedures, data sources and analysis, 2009.

Anticamara, J., Watson, R., Gelchu, A., and Pauly, D.: Global fishing effort (1950–2010): trends, gaps, and implications, Fisheries Research, 107, 131–136, 2011.

Behrenfeld, M. J. and Falkowski, P. G.: Photosynthetic rates derived from satellite-based chlorophyll concentration, Limnology and Oceanography, 42, 1–20, 1997.

Bianchi, D., Carozza, D. A., Galbraith, E. D., Guiet, J., and DeVries, T.: Estimating global biomass and biogeochemical cycling of marine fish with and without fishing, Science advances, 7, eabd7554, 2021.

Blanchard, J. L., Jennings, S., Holmes, R., Harle, J., Merino, G., Allen, J. I., Holt, J., Dulvy, N. K., and Barange, M.: Potential consequences of climate change for primary production and fish production in large marine ecosystems, Philosophical Transactions of the Royal Society of London B: Biological Sciences, 367, 2979–2989, https://doi.org/10.1098/rstb.2012.0231, 2012.

Brown, J. H., Gillooly, J. F., Allen, A. P., Savage, V. M., and West, G. B.: Toward a metabolic theory of ecology, Ecology, 85, 1771–1789, 2004.

Buesseler, K. O. and Boyd, P. W.: Shedding light on processes that control particle export and flux attenuation in the twilight zone of the open ocean, Limnology and Oceanography, 54, 1210–1232, 2009.

Carozza, D. A., Bianchi, D., and Galbraith, E. D.: The ecological module of BOATS-1.0: a bioenergetically constrained model of marine upper trophic levels suitable for studies of fisheries and ocean biogeochemistry, Geoscientific Model Development, 9, 1545–1565, 2016.

Carozza, D. A., Bianchi, D., and Galbraith, E. D.: Formulation, General Features and Global Calibration of a Bioenergetically-Constrained Fishery Model, PLOS One, 12, 1–28, https://doi.org/10.1371/journal.pone.0169763, 2017.

Carozza, D. A., Bianchi, D., and Galbraith, E. D.: Metabolic impacts of climate change on marine ecosystems: Implications for fish communities and fisheries, Global Ecology and Biogeography, 28, 158–169, 2019.

Carr, M.-E., Friedrichs, M. A., Schmeltz, M., Aita, M. N., Antoine, D., Arrigo, K. R., Asanuma, I., Aumont, O., Barber, R., Behrenfeld, M., et al.: A comparison of global estimates of marine primary production from ocean color, Deep Sea Research Part II: Topical Studies in Oceanography, 53, 741–770, 2006.

Du Pontavice, H., Gascuel, D., Reygondeau, G., Maureaud, A., and Cheung, W. W.: Climate change undermines the global functioning of marine food webs, Global Change Biology, 26, 1306–1318, 2020.

Dunne, J. P., Armstrong, R. A., Gnanadesikan, A., and Sarmiento, J. L.: Empirical and mechanistic models for the particle export ratio, Global Biogeochemical Cycles, 19, 2005.

Eddy, T. D., Bernhardt, J. R., Blanchard, J. L., Cheung, W. W., Colléter, M., Du Pontavice, H., Fulton, E. A., Gascuel, D., Kearney, K. A., Petrik, C. M., et al.: Energy Flow Through Marine Ecosystems: Confronting Transfer Efficiency, Trends in Ecology & Evolution, 2020.

Fredston, A. L., Cheung, W. W., Frölicher, T. L., Kitchel, Z. J., Maureaud, A. A., Thorson, J. T., Auber, A., Mérigot, B., Palacios-Abrantes, J., Palomares, M. L. D., et al.: Marine heatwaves are not a dominant driver of change in demersal fishes, Nature, pp. 1–6, 2023.

Galbraith, E. D., Carozza, D. A., and Bianchi, D.: A coupled human-Earth model perspective on long-term trends in the global marine fishery, Nature Communications, 8, 14 884, http://dx.doi.org/10.1038/ncomms14884, 2017.

Galbraith, E. D., Le Mézo, P., Solanes Hernandez, G., Bianchi, D., and Kroodsma, D.: Growth limitation of marine fish by low iron availability in the open ocean, Frontiers in Marine Science, p. 509, 2019.

https://doi.org/10.5194/gmd-2024-26
Preprint. Discussion started: 2 May 2024

Gascuel, D., Guénette, S., and Pauly, D.: The trophic-level-based ecosystem modelling approach: theoretical overview and practical uses, ICES Journal of Marine Science, 68, 1403–1416, 2011.

Guiet, J., Galbraith, E., Bianchi, D., and Cheung, W.: Bioenergetic influence on the historical development and decline of industrial fisheries, ICES Journal of Marine Science, 77, 1854–1863, 2020.

Hatton, I. A., Dobson, A. P., Storch, D., Galbraith, E. D., and Loreau, M.: Linking scaling laws across eukaryotes, Proceedings of the National Academy of Sciences, 116, 21 616–21 622, 2019.

Hatton, I. A., Heneghan, R. F., Bar-On, Y. M., and Galbraith, E. D.: The global ocean size spectrum from bacteria to whales, Science Advances, 7, eabh3732, https://doi.org/10.1126/sciadv.abh3732, 2021.

Heneghan, R. F., Everett, J. D., Sykes, P., Batten, S. D., Edwards, M., Takahashi, K., Suthers, I. M., Blanchard, J. L., and Richardson, A. J.: A functional size-spectrum model of the global marine ecosystem that resolves zooplankton composition, Ecological Modelling, 435, 109 265, 2020.

Heneghan, R. F., Galbraith, E., Blanchard, J. L., Harrison, C., Barrier, N., Bulman, C., Cheung, W., Coll, M., Eddy, T. D., Erauskin-Extramiana, M., et al.: Disentangling diverse responses to climate change among global marine ecosystem models, Progress in Oceanography, 198, 102 659, 2021.

Hidalgo, M. and Browman, H. I.: Developing the knowledge base needed to sustainably manage mesopelagic resources, 2019.

Irigoien, X., Klevjer, T. A., Røstad, A., Martinez, U., Boyra, G., and et al., A. J. L.: Large mesopelagic fishes biomass and trophic efficiency in the open ocean, Nature Communications, 5, 2014.

Jennings, S. and Collingridge, K.: Predicting consumer biomass, size-structure, production, catch potential, responses to fishing and associated uncertainties in the world's marine ecosystems, PloS one, 10, e0133 794, 2015.

Kaartvedt, S., Staby, A., and Aksnes, D. L.: Efficient trawl avoidance by mesopelagic fishes causes large underestimation of their biomass, Marine Ecology Progress Series, 456, 1–6, 2012.

Kerry, C. R., Exeter, O. M., and Witt, M. J.: Monitoring global fishing activity in proximity to seamounts using automatic identification systems, Fish and Fisheries, 23, 733–749, 2022.

Kooijman, S. A. L. M.: Dynamic Energy and Mass Budgets in Biological Systems, Cambridge University Press, third edn., ISBN 9780511565403, http://dx.doi.org/10.1017/CBO9780511565403, cambridge Books Online, 2010.

Kroodsma, D. A., Mayorga, J., Hochberg, T., Miller, N. A., Boerder, K., Ferretti, F., Wilson, A., Bergman, B., White, T. D., Block, B. A., et al.: Tracking the global footprint of fisheries, Science, 359, 904–908, 2018.

Lam, V. W. Y., Sumaila, U. R., Dyck, A., Pauly, D., and Watson, R.: Construction and first applications of a global cost of fishing database, ICES Journal of Marine Science, 68, 1996–2004, https://doi.org/10.1093/icesjms/fsr121, 2011.

Le Mézo, P., Guiet, J., Scherrer, K., Bianchi, D., and Galbraith, E.: Global nutrient cycling by commercially targeted marine fish, Biogeosciences, 19, 2537–2555, 2022.

Le Mézo, P. K. and Galbraith, E. D.: The fecal iron pump: global impact of animals on the iron stoichiometry of marine sinking particles, Limnology and Oceanography, 66, 201–213, 2021.

Locarnini, R. A., Mishonov, A. V., Antonov, J. I., Boyer, T. P., and Garcia, H. E.: World Ocean Atlas 2005, Volume 1: Temperature. S. Levitus, Ed. NOAA Atlas NESDIS 61, U.S. Government Printing Office, Washington, D.C., 182 pp, 2006.

Lotze, H. K., Tittensor, D. P., Bryndum-Buchholz, A., Eddy, T. D., Cheung, W. W. L., Galbraith, E. D., Barange, M., Barrier, N., Bianchi, D., Blanchard, J. L., Bopp, L., Büchner, M., Bulman, C. M., Carozza, D. A., Christensen, V., Coll, M., Dunne, J. P., Fulton, E. A., Jennings, S., Jones, M. C., Mackinson, S., Maury, O., Niiranen, S., Oliveros-Ramos, R., Roy, T., Fernandes, J. A., Schewe, J., Shin,

https://doi.org/10.5194/gmd-2024-26
Preprint. Discussion started: 2 May 2024

Y.-J., Silva, T. A. M., Steenbeek, J., Stock, C. A., Verley, P., Volkholz, J., Walker, N. D., and Worm, B.: Global ensemble projections reveal trophic amplification of ocean biomass declines with climate change, Proceedings of the National Academy of Sciences, https://doi.org/10.1073/pnas.1900194116, 2019.

Marra, J., Trees, C. C., and O'Reilly, J. E.: Phytoplankton pigment absorption: a strong predictor of primary productivity in the surface ocean, Deep Sea Research Part I: Oceanographic Research Papers, 54, 155–163, 2007.

Martin, J. H., Knauer, G. A., Karl, D. M., and Broenkow, W. W.: VERTEX: carbon cycling in the northeast Pacific, Deep Sea Research Part A. Oceanographic Research Papers, 34, 267–285, 1987.

Maureaud, A., Fredston, A., Guralnick, R., Abrantes, J. P., Palomares, M. D., Pinsky, M., Shackell, N., Thorson, J. T., Merigot, B., et al.: FISHGLOB: a collaborative infrastructure for marine science and management, 2023.

Maury, O.: An overview of APECOSM, a spatialized mass balanced "Apex Predators ECOSystem Model" to study physiologically structured tuna population dynamics in their ecosystem, Progress in Oceanography, 84, 113–117, 2010.

Maury, O. and Poggiale, J.-C.: From individuals to populations to communities: A dynamic energy budget model of marine ecosystem size-spectrum including life history diversity, Journal of Theoretical Biology, 324, 52 – 71, https://doi.org/http://dx.doi.org/10.1016/j.jtbi.2013.01.018, 2013.

Morato, T., Cheung, W., and Pitcher, T.: Vulnerability of seamount fish to fishing: fuzzy analysis of life-history attributes, Journal of Fish Biology, 68, 209–221, 2006.

Palomares, M. L. and Pauly, D.: On the creeping increase of vessels' fishing power, Ecology and Society, 24, 2019.

Pauly, D. and Zeller, D.: Catch reconstructions reveal that global marine fisheries catches are higher than reported and declining, Nature Communications, 7, 10 244, 2016.

Pauly, D., Zeller, D., and Palomares, M.: Sea Around Us Concepts, Design and Data, seaaroundus.org, 2020.

Petrik, C. M., Stock, C. A., Andersen, K. H., van Denderen, P. D., and Watson, J. R.: Bottom-up drivers of global patterns of demersal, forage, and pelagic fishes, Progress in oceanography, 176, 102 124, 2019.

Ricard, D., Minto, C., Jensen, O. P., and Baum, J. K.: Examining the knowledge base and status of commercially exploited marine species with the RAM Legacy Stock Assessment Database, Fish and fisheries, 13, 380–398, 2012.

Rousseau, Y., Watson, R. A., Blanchard, J. L., and Fulton, E. A.: Evolution of global marine fishing fleets and the response of fished resources, Proceedings of the National Academy of Sciences, 116, 12 238–12 243, https://doi.org/10.1073/pnas.1820344116, 2019.

Rousseau, Y., Blanchard, J. L., Novaglio, C., Pinnell, K. A., Tittensor, D. P., Watson, R. A., and Ye, Y.: A database of mapped global fishing activity 1950–2017, Scientific Data, 11, 48, 2024.

Ryther, J. H.: Photosynthesis and Fish Production in the Sea, Science, 166, 72–76, https://doi.org/10.1126/science.166.3901.72, 1969.

Sala, E., Mayorga, J., Costello, C., Kroodsma, D., Palomares, M. L., Pauly, D., Sumaila, U. R., and Zeller, D.: The economics of fishing the high seas, Science advances, 4, eaat2504, 2018.

Scherrer, K. and Galbraith, E.: Regulation strength and technology creep play key roles in global long-term projections of wild capture fisheries, ICES Journal of Marine Science, https://doi.org/10.1093/icesjms/fsaa109, fsaa109, 2020.

Scherrer, K. J., Harrison, C. S., Heneghan, R. F., Galbraith, E., Bardeen, C. G., Coupe, J., Jägermeyr, J., Lovenduski, N. S., Luna, A., Robock, A., et al.: Marine wild-capture fisheries after nuclear war, Proceedings of the National Academy of Sciences, 117, 29 748–29 758, 2020.

St. John, M. A., Borja, A., Chust, G., Heath, M., Grigorov, I., Mariani, P., Martin, A. P., and Santos, R. S.: A dark hole in our understanding of marine ecosystems and their services: perspectives from the mesopelagic community, Frontiers in Marine Science, 3, 31, 2016.

https://doi.org/10.5194/gmd-2024-26
Preprint. Discussion started: 2 May 2024

Stock, C. A., John, J. G., Rykaczewski, R. R., Asch, R. G., Cheung, W. W. L., Dunne, J. P., Friedland, K. D., Lam, V. W. Y., Sarmiento, J. L., and Watson, R. A.: Reconciling fisheries catch and ocean productivity, Proceedings of the National Academy of Sciences, 114, E1441–E1449, https://doi.org/10.1073/pnas.1610238114, 2017.

Sumaila, U. R., Marsden, A. D., Watson, R., and Pauly, D.: A global ex-vessel fish price database: construction and applications, Journal of Bioeconomics, 9, 39–51, 2007.

Sumaila, U. R., Lam, V. W., Miller, D. D., Teh, L., Watson, R. A., Zeller, D., Cheung, W. W., Côté, I. M., Rogers, A. D., Roberts, C., et al.: Winners and losers in a world where the high seas is closed to fishing, Scientific Reports, 5, 1–6, 2015.

Swartz, W., Sala, E., Tracey, S., Watson, R., and Pauly, D.: The spatial expansion and ecological footprint of fisheries (1950 to present), PLOS One, 5, e15 143, 2010.

Tagliabue, A., Bowie, A. R., Boyd, P. W., Buck, K. N., Johnson, K. S., and Saito, M. A.: The integral role of iron in ocean biogeochemistry, Nature, 543, 51–59, 2017.

Tittensor, D. P., Mora, C., Jetz, W., Lotze, H. K., Ricard, D., Berghe, E. V., and Worm, B.: Global patterns and predictors of marine biodiversity across taxa, Nature, 466, 1098–1101, 2010.

Tittensor, D. P., Novaglio, C., Harrison, C. S., Heneghan, R. F., Barrier, N., Bianchi, D., Bopp, L., Bryndum-Buchholz, A., Britten, G. L., Büchner, M., et al.: Next-generation ensemble projections reveal higher climate risks for marine ecosystems, Nature Climate Change, 11, 973–981, 2021.

van Denderen, D., Gislason, H., van den Heuvel, J., and Andersen, K. H.: Global analysis of fish growth rates shows weaker responses to temperature than metabolic predictions, Global Ecology and Biogeography, 29, 2203–2213, 2020.

van Denderen, D., Maureaud, A. A., Andersen, K. H., Gaichas, S., Lindegren, M., Petrik, C. M., Stock, C. A., and Collie, J.: Demersal fish biomass declines with temperature across productive shelf seas, Global Ecology and Biogeography, 2023.

van Denderen, P. D., Lindegren, M., MacKenzie, B. R., Watson, R. A., and Andersen, K. H.: Global patterns in marine predatory fish, Nature ecology & evolution, 2, 65, 2018.

van Denderen, P. D., Petrik, C. M., Stock, C. A., and Andersen, K. H.: Emergent global biogeography of marine fish food webs, Global Ecology and Biogeography, 30, 1822–1834, 2021.

Watson, R. A.: A database of global marine commercial, small-scale, illegal and unreported fisheries catch 1950–2014, Scientific Data, 4, 2017.

Watson, R. A. and Morato, T.: Fishing down the deep: Accounting for within-species changes in depth of fishing, Fisheries Research, 140, 63–65, 2013.

Weber, T., Cram, J. A., Leung, S. W., DeVries, T., and Deutsch, C.: Deep ocean nutrients imply large latitudinal variation in particle transfer efficiency, Proceedings of the National Academy of Sciences, 113, 8606–8611, 2016.

Worm, B. and Branch, T. A.: The future of fish, Trends in Ecology & Evolution, 27, 594 – 599, https://doi.org/https://doi.org/10.1016/j.tree.2012.07.005, 2012.

Worm, B., Hilborn, R., Baum, J. K., Branch, T. A., Collie, J. S., Costello, C., Fogarty, M. J., Fulton, E. A., Hutchings, J. A., Jennings, S., et al.: Rebuilding global fisheries, Science, 325, 578–585, 2009.

Zwolinski, J. P., Demer, D. A., Byers, K. A., Cutter, G. R., Renfree, J. S., Sessions, T. S., and Macewicz, B. J.: Distributions and abundances of Pacific sardine (Sardinops sagax) and other pelagic fishes in the California Current Ecosystem during spring 2006, 2008, and 2010, estimated from acoustic–trawl surveys, Fishery Bulletin, 110, 110–122, 2012.